Volume 6
Number 5
May 2021
Pages 749–946

Reaction Chemistry & Engineering

Linking fundamental chemistry and engineering to create scalable, efficient processes

rsc.li/reaction-engineering

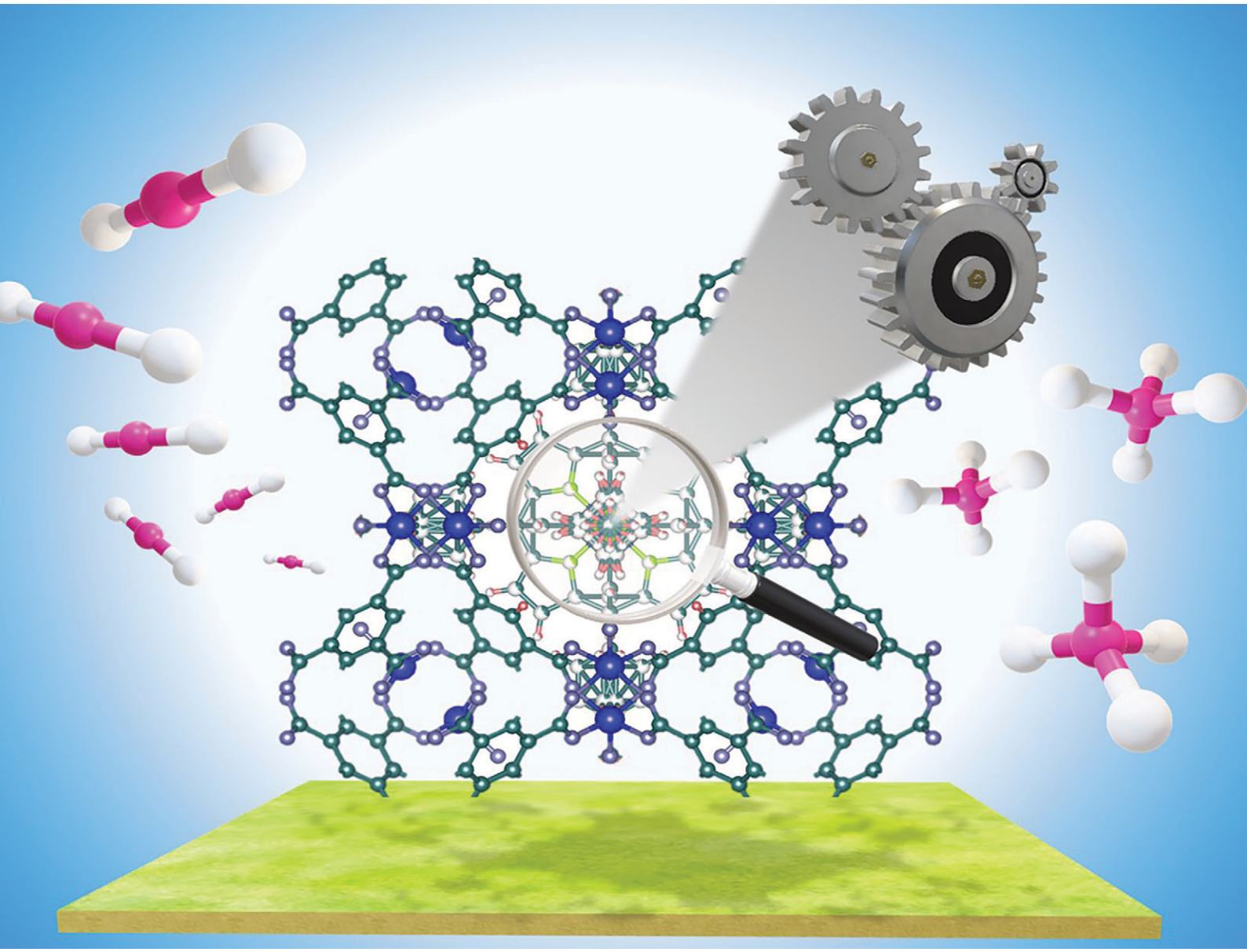

ISSN 2058-9883

ROYAL SOCIETY OF CHEMISTRY

REVIEW ARTICLE

J. Gandara-Loe, T. R. Reina *et al.*

Understanding the opportunities of metal–organic frameworks (MOFs) for CO_2 capture and gas-phase CO_2 conversion processes: a comprehensive overview

Reaction Chemistry & Engineering

ROYAL SOCIETY OF CHEMISTRY

REVIEW

View Article Online
View Journal | View Issue

Cite this: *React. Chem. Eng.*, 2021, **6**, 787

Understanding the opportunities of metal–organic frameworks (MOFs) for CO_2 capture and gas-phase CO_2 conversion processes: a comprehensive overview

J. Gandara-Loe,*[a] L. Pastor-Perez,[ab] L. F. Bobadilla,[a] J. A. Odriozola[ab] and T. R. Reina *[ab]

Received 25th January 2021,
Accepted 13th March 2021

DOI: 10.1039/d1re00034a

rsc.li/reaction-engineering

The rapid increase in the concentration of atmospheric carbon dioxide is one of the most pressing problems facing our planet. This challenge has motivated the development of different strategies not only in the reduction of CO_2 concentrations *via* green energy alternatives but also in the capture and conversion of CO_2 into value-added products. Metal–organic frameworks (MOFs) are a relatively new class of porous materials with unique structural characteristics such as high surface areas, chemical tunability and stability, and have been extensively studied as promising materials to address this challenge. This comprehensive review identifies the specific structural and chemical properties of MOFs that result in advanced CO_2 capture capacities and fairly encouraging catalytic CO_2 conversion behaviour. More importantly, we describe an interconnection among the unique properties of MOFs and the engineering aspects of these intriguing materials towards CO_2 capture and conversion processes.

1. Introduction

Climate change is an alarming problem that has motivated the development of strategies not only in the replacement of

[a] *Department of Inorganic Chemistry, University of Seville, 41092, Seville, Spain. E-mail: jgloe@us.es*
[b] *Chemical & Process Engineering Department, University of Surrey, Guildford GU2 7XH, UK. E-mail: t.ramirezreina@surrey.ac.uk*

Jesus Gandara-Loe

Jesus Gandara-Loe is a Postdoctoral Researcher at the University of Seville (Spain). He obtained his PhD degree in Materials Science from the University of Alicante (Spain) in 2020. His research interests encompass metal–organic frameworks (MOFs), gas adsorption in highly porous materials, hydrocarbon separation, drug delivery using porous materials, and structural characterization of porous materials using high sensitivity techniques.

Laura Pastor-Pérez

Laura Pastor-Pérez is an Assistant Professor at the Inorganic Chemistry Department at the University of Seville (Spain). Currently, she is also working as a Visiting Research Fellow at the Department of Chemical and Process Engineering at the University of Surrey (UK). Dr Pastor-Perez received her PhD degree in Materials Science from the University of Alicante (Spain) in 2016. For her thesis work she received the extraordinary award of the Spanish Royal Society of Chemistry. Her research interests include the development (synthesis and characterization) of advanced heterogeneous catalysts, mainly supported metal catalysts and carbon-based materials for the production of clean energy and sustainability. Nowadays, her efforts are focused on biomass valorisation, clean hydrogen production and chemical CO_2 recycling.

conventional fossil fuels by renewable alternatives but also in the reduction of greenhouse gas emissions (mainly CO_2 coming from fossil fuel power plants) and mitigation of climate change *via* CO_2 capture and conversion into value-added products.

CO_2 capture at an industrial level is a direct technology based on the chemical absorption of CO_2.[1] The conventional amine-based absorption technology has been implemented on a large commercial scale as a direct strategy to curb industrial carbon dioxide emission.[2] Nevertheless, this process presents inconveniences such as harmful effects of the toxic volatiles, corrosion, hazardous by-products, solvent loss, and most importantly, high energy penalties for the regeneration process.[3] Hence, new alternatives such as CO_2 adsorption in porous materials are gaining attention for different applications.[4]

Luis F. Bobadilla

Dr Luis F. Bobadilla received his PhD degree in Materials Science from the University of Seville (Spain) in 2011, where he is currently an Assistant Professor in Inorganic Chemistry from 2018. His research interests are focused on the rational design of heterogeneous catalysts and catalytic process optimization aided by in situ and operando spectroscopic methods. He has co-authored over 40 journal articles, two patents and co-edited and contributed to six books.

Within the spectra of porous materials, metal–organic frameworks (MOFs) have emerged as a new class of crystalline porous materials with exceptional structural characteristics.[5] MOFs are crystalline materials formed through strong interactions between metal ions or clusters and coordinated ligands, forming one-, two-, or three-dimensional porous structures (Fig. 1).[6,7] These materials show an almost infinite number of combinations between organic and inorganic building blocks, offering enormous flexibility in terms of pore size, structure, and shape.[8] Characteristics such as ultrahigh porosity (up to 90% free volume), thermal and structural stability, *etc.* make them of increasing interest for potential application in gas storage, catalysis, membranes, thin-film devices, gas separation, biomedical imaging, and drug delivery.[9]

The structural versatility of MOFs (*e.g.* structural tunability, control of surface chemistry, control of pore size and shape, and composite synthesis capability) has allowed exploring these materials not only as potential platforms to capture CO_2 but also as promising catalysts for CO_2 conversion.[10–12] Several strategies have been employed to finely tune the structures of MOFs, including the incorporation of open metal sites, amine functional groups, structural flexibility or framework interpenetration. These remarkable structural tunability and chemical functionality are enormously different from those of other porous materials such as zeolites and activated carbons, allowing the direct optimization of pore structures, surface functions, and other properties for specific applications. Additionally, MOFs often exhibit a higher pore volume and surface area than zeolites and activated carbons. CO_2 adsorption and separation in MOFs have been studied intensively through experimental techniques and computational simulation methods in the past decade.[13]

José A. Odriozola

Prof. José A. Odriozola is a Full Professor at the Inorganic Chemistry Department and the Materials Science Institute at the University of Seville, Spain, and a Visiting Professor at the Chemical Engineering Department of the University of Surrey, UK. His research interests include development of catalysts and catalytic processes, as well as catalytic processes from "electrons to reactors". He has co-edited Heterogeneous Catalysis for Energy Applications (with T. R. Reina, 2020) and Engineering Solutions for CO_2 Conversion (with H. García-Arellano and T. R. Reina, 2020).

Tomas R. Reina

Dr. Tomas R. Reina, PhD, FHEA, AMIChemE, received his PhD degree in Chemistry from the University of Seville (Spain) in 2014 and then he moved to the UK where he has developed his career as the Catalysis & Reaction Engineering Group Leader at the Department of Chemical & Process Engineering at the University of Surrey. He is a Visiting Professor at the HUST (China, 2019), an academic member of the DICP-Surrey Joint Centre for Future Materials and a Low-Carbon Energy Fellow at the University of Seville. His research interests include the development of advanced heterogeneous catalysts for energy and sustainability. In particular, his work is focused on clean hydrogen production, carbon dioxide utilisation and biomass valorisation.

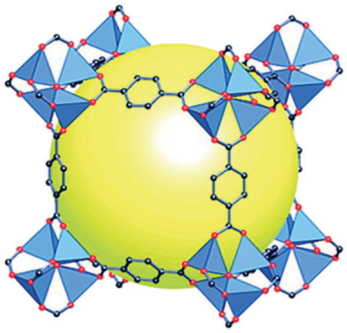

Fig. 1 Scheme of a MOF structure (MOF-5) formed from tetrametallic SBUs (blue polyhedra) linked to terephthalic acid, with a cavity (yellow sphere) shown to capture gas/liquid molecules (reproduced from ref. 7 with permission from the American Chemical Society, copyright 2021).

The main challenge of CO_2 catalytic conversion processes relies on the CO_2 chemical inertness and thermodynamic stability of CO_2 which typically require aggressive reaction conditions such as high temperature and high pressure, which, by consequence, are highly energy-intensive and environmentally unacceptable. Therefore, the conversion of CO_2 under mild conditions requires the activation of CO_2 with a highly efficient and selective catalyst such as metal–organic frameworks (MOFs). MOFs have been reported as promising candidates for CO_2 capture and efficient catalysts due to their ultra-high porosity, crystallinity, and tuneable organic linkers resulting in materials with unique properties such as high surface area, high stability, open channels, and permanent porosity. MOFs therefore frequently take the edge over other adsorbents and catalysts for C1 chemistry and in particular for highly effective CO_2 capture and CO_2 conversion processes.[14]

To date, many reports related to CO_2 capture and conversion have focused on the advances in the structural and molecular factors controlling the processes. However, in this review, we combine the main advances related to structural strategies to improve CO_2 capture and conversion with key engineering affecting the large-scale application of these materials.

2. Synthesis approach and structural features of metal–organic frameworks

As a result of the large number of linkers available in the market and the high number of possible combinations in the synthesis of MOFs, in the last decade, there has been an exponential growth in the number of new MOF structures described in the literature.

Synthesis optimization of MOFs is an essential step to obtain materials with desirable characteristics such as specific surface area and crystal morphology. Hence, different methods of MOF synthesis have been developed to fulfil these needs. As depicted in Fig. 2, MOF synthesis methods generally comprise conventional methods, *i.e.*, those carried out by conventional electrical heating taking place in closed vessels under autogenous pressure above or below the boiling point of the solvent.[15] Compared to the conventional methods, high-throughput methods (HT) which are closely connected with the concepts of automation, parallelization, and miniaturization have shown to be an ideal tool to investigate the MOF formation parameters, such as compositional (*i.e.*, molar ratios of starting materials, pH, solvent, *etc.*) and process parameters (*i.e.*, reaction time, temperature, and pressure) in a serial way.[16] Alternatively to the conventional methods where the energy is generally

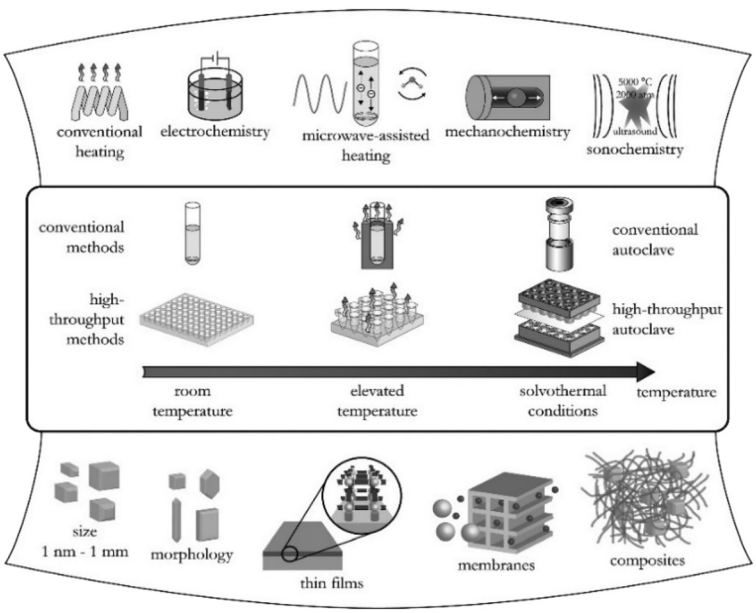

Fig. 2 Overview of synthesis methods, possible reaction temperatures, and final reaction products in MOF synthesis (reproduced from ref. 16 with permission from the American Chemical Society, copyright 2021).

introduced through conventional electric heating, energy can also be introduced through other means, for example, by an electric potential, electromagnetic radiation, mechanical waves (ultrasound), or mechanically.

The solvothermal synthesis of MOFs is one of the most widely used methods due to its facile implementation and relatively favoured up-scaling. Parameters such as the metal/ligand ratio, solvent, modulating reagent, and temperature affect the shape and size (growth) of the crystals greatly. A wide number of MOFs such as ZIFs,[17] HKUST-1,[18] UiO-66,[19] and UiO-67[20] have been synthesized for the first time using this method.

The microwave-assisted (MW) synthesis of MOFs is mainly focused on i) the acceleration of the crystallization, ii) nanoscale products, and most importantly iii) improving the porosity and the selectivity of polymorphs. One of the first examples of MW-assisted MOF synthesis was reported by Jhung *et al.* for Cr-MIL-100. In this synthesis, the solution of metallic salts and ligands was sealed in a Teflon autoclave and kept in an MW oven at 220 °C for 1, 2, and 4 h obtaining crystals with different shapes and sizes.[21]

In the electrochemical synthesis of MOFs, the metal cations diffuse to the reaction media through the anode, and the organic linkers are dissolved in the electrolyte, where they react with the anode. The advantage of the electrochemical synthesis of MOFs over other methods is the exclusion of anions coming from the metallic salts (*i.e.*, chloride, nitrate, sulphate, *etc.*), which has been demonstrated to be beneficial for large scale production.[16] A wide number of different MOF films and patterned coatings have been studied using this synthesis method.[22]

Mechanochemistry offers a green route for MOF production which is of great interest due to its advantages in comparison with other synthesis routes such as being solvent-free (or minimal amount of solvent), having short reaction times and without requiring external heat supply.[23] However, the first limitation lies in the scaling-up of the synthesis; for instance, it can be classified as a batch processing technique with a low production yield. Herein, it is important to mention that a purification step must be added despite the solvent-free nature of this synthesis strategy.[24,25]

In sonochemical synthesis, cavitation promotes an intimate interaction between molecules and energy. For instance, the pressure and temperature in the hot spot of the bubble may reach 1000 bar and 5000 K (with heating and cooling rates of 10^{10} K s^{-1}), respectively. Using sonochemistry to synthesize MOFs presents advantages of having a short synthesis time, being environmentally friendly, and being a high optimum energy-efficient process.[16] The first MOF reported to be synthesized using sonochemistry was Zn–BTC, which consisted of MOF nanocrystals synthesized at room temperature and atmospheric pressure in 20% ethanol/water under ultrasound irradiation.[26]

Irrespective of the synthesis route, MOFs have provided unique opportunities for a wide number of applications. Due to their excellent physicochemical properties mentioned before, these materials have been applied in drug delivery, catalysis, sensor technology, gas storage and separation, water sorption applications, electrical energy storage, and luminescent materials, among many other advanced technologies.[27]

When low-carbon technologies are considered, MOFs serve as promising materials for CO_2 capture and conversion due to their unique advantages such as (a) predictable and functionalizable structures, *i.e.* MOF structures can be easily predicted, and the structure can not only be designed as required, but can also be tuned. (b) Hybrid structures: MOFs are highly compatible with other materials to synthesize MOF composites. (c) Particular strengths for catalysis, such as high catalytic efficiency, facile separation and reusability. (d) The structural characteristics of MOFs allow a straightforward understanding of the structure–activity relationship, which ultimately helps to improve the materials and process design further.[28]

3. CO_2 capture in MOFs

Presently mature technologies for CO_2 capture at an industrial level are based on aqueous amine scrubbing; however, this technology involves a huge industrial separation process that is expensive and highly energy-intensive.[14,29] CO_2 capture using porous materials is gaining attention in different applications.[30] Considering the extremely high surface area and the physicochemical surface properties thereof, the use of MOFs can serve as an alternative approach to reduce the energy penalty associated with CO_2 capture due to their high porosity and chemical tunability.[31–34] For instance, the use of different ligands can easily control the pore shape and size in MOFs, which is an essential requirement to have a preferential selectivity to CO_2 over other similar molecules (H_2, N_2 and CH_4).[35] Different strategies have been developed to enhance and control the adsorption and capture of CO_2 into the inner pores of MOFs, which are mostly related to the composition of ligands or post-synthesis modification of the frameworks. Table 1 summarises some of the most relevant CO_2 capture amounts in MOFs with a variety of ligands and metals.

3.1. Factors influencing CO_2 capture in MOFs

CO_2 adsorbed in porous materials (*i.e.* zeolites, silicas, polymers, and active carbons) is attached physically through weak interaction between CO_2 and the pore. However, MOFs also capture CO_2 by physisorption; their ultra-high surface areas give much higher uptake capacities compared to other materials. As depicted in Fig. 3, the ability to design MOFs that possess features such as open metal sites (OMSs), Lewis basic sites (LBSs), covalent-bound polar functional groups, tunable pore sizes, framework flexibility, or hydrophobicity has attracted enormous attention for CO_2 capture.[28]

3.1.1. MOFs with open metal sites (OMSs). The open metal sites (OMSs) in MOFs are generated due to the evacuation of the coordinated solvent molecules in the framework (*e.g.*,

Table 1 Summary of MOF-based adsorbents and the corresponding CO_2 capture capacity for each material

Adsorbent	Capacity[a] (mmol g^{-1})	Temperature (K)	Pressure (bar)	Ref.
JUC-150	0.9	298	1	33
MOF-2	0.6	298	1	39
Norit RB	2.5	298	1	39
MOF-505	3.3	298	1.1	39
MOF-74(Zn)	4.9	298	1.1	39
$Cu_3(BTC)_2$	4.1	298	1	39
IRMOF-11	1.8	298	1.1	39
IRMOF-3	1.2	298	1.1	39
IRMOF-6	1.1	298	1.2	39
IRMOF-1	1.1	298	1.1	39
MOF-177	0.8	298	1	39
MIL-100 (Cr)	5.5	303	10	40
Mg-MOF-74	9	298	1	42
Ni-MOF-74	6.8	298	1	42
Fe-MOF-74	6.8	298	1	42
Co-MOF-74	6.6	298	1	42
Zn-MOF-74	6	298	1	42
Mn-MOF-74	5.9	298	1	42
Cu-MOF-74	3	298	1	42
LIMF-26	3.1	298	1	44
NU-100	2.7	298	1	46
PCN-61	23.5	298	35	47
PCN-66	26.3	298	35	47
PCN-68	30.4	298	35	47
MIL-96(Al)	5.2	303	20	48
UTSA-20	5.4	303	1	49
MIL-102(Cr)	3.5	304	30	50
UiO-66 (Zr)	7.8	303	20	53
UiO-66(Zr)-NH_2	8	303	35	53
$Mg_2(dobdc)(N_2H_4)_{1.8}$	5.5	298	1	54
MIL-53 (Al)	6.8	303	30	55
Bio-MOF-11	4	298	1	59
Cu-TDPAT	6.1	298	1	60
Cu-BTTri	3.7	298	1	61
ZnF(daTZ)	3.3	298	1	64
ZnF(aTZ)	3.1	298	1	64
ZnF(TZ)	2.7	298	1	64
ZIF-68	1.8	298	1	65
ZIF-69	2.2	298	1	65
ZIF-70	1.3	298	1	65
ZIF-78	2.7	298	1	65
ZIF-79	1.6	298	1	65
ZIF-81	2.2	298	1	65
ZIF-82	2.2	298	1	65
TMOF-1	1	298	1	66
MUF-15	3.6	298	1	67
ZIF-7	5	195	1	78
NOTT-202a	12	298	30	80
CALF-33-Et3	0.5	293	1	90
CALF-33-Et2H	1.1	293	1	90
Ni-DOBCO	5	298	1	91
MOF-5	1	298	1	92
ZIF-300	1.3	298	1	94
ZIF-301	1.2	298	1	94
ZIF-302	0.1	298	1	94
SNU-100	3.2	298	1	111
MIL-53 (Cr)	10.2	303	25	124

[a] Some of the CO_2 adsorption capacities have been converted to these units from the originally reported units.

H_2O, DMF, ethanol) that serve as terminal ligands, using heating or vacuum. The role of the OMSs in MOFs has been proved to be of high importance in improving their CO_2 capture properties due to the great affinity of OMSs toward CO_2 through a dipole–quadrupole interaction which inherently impacts the separation selectivity.[36–38] These OMSs often work as Lewis acid sites (LASs) that have been shown to coordinate to CO_2.

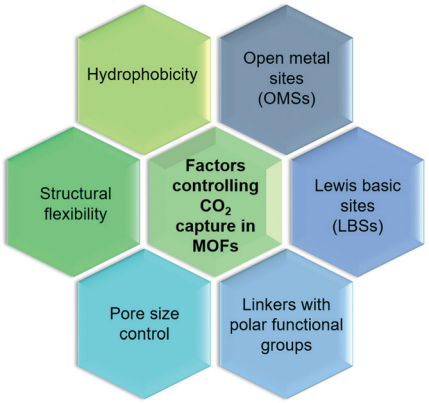

Fig. 3 Factors controlling the CO_2 capture performance in MOFs.

HKUST-1 or Cu_3(benzene-1,3,5-tricarboxylate or BTC)$_2$ has been one of the first MOFs identified with OMSs, successfully studied in CO_2 capture at either low pressure (up to 1 bar) or high pressure (up to 40 bar). For instance, Millward *et al.* reported HKUST-1 CO_2 uptake capacity of about 10 mmol g^{-1} at 42 bar and ambient temperature, which is an exceptional value reached for this type of material.[39] Recently, a computational study based on DFT and energy minimization principle was conducted to understand the interactions of CO_2 with HKUST-1, which produced results in good agreement with previous experimental data indicating the appropriateness of computational methods as a potential means for the screening of MOFs for CO_2 separation.[40,41]

Among all MOFs, those sharing the same ligand or the so-called isostructural MOFs have attracted considerable attention as a consequence of their extraordinary CO_2 capture capacity. The family of isostructural MOFs based on 2,5-dihydroxyterephthalic acid (DOBDC), also known as M-MOF-74 or M-CPO-27 (M = Mg^{2+}, Ni^{2+}, Co^{2+}, Zn^{2+}) composed of an array of one-dimensional hexagonal channels with OMSs at the secondary building units (SBUs), has become one of the most well-studied sets of MOFs for CO_2 capture due to their extraordinary CO_2 uptake capacities at low pressures.[42–44] The main limitation of OMSs–MOFs for CO_2 capture leads to their ineffectiveness in the presence of water due to the stronger binding interactions of water than CO_2, thus limiting the effectiveness of such materials for CO_2 capture from flue gas streams.[45]

Following this work, a wide variety of MOFs bearing OMSs have been applied as CO_2 adsorbents, including NU-1000, MIL-101, and PCN-68 offering plenty of opportunities for CO_2 capture.[46–50]

3.1.2. MOFs with Lewis basic sites (LBSs). As mentioned in the previous section, the use of metallic SBUs with certain features can benefit the CO_2 sorption and selectivity capacity of MOFs. Additionally, the ligand composition also plays an important role as an agent of improvement. For instance, a strategy used in the industrial separation of CO_2 using aqueous amine solution such as monoethanolamide (MEA)[29,51] has inspired the addition of Lewis basic amine sites (LBSs) into MOFs which has been proved to impact the CO_2 adsorption capacity significantly.[39,52–55] Such adsorption capacity boosting is the consequence of the interactions between the localized dipoles of the N-containing groups and the quadrupole moment of CO_2, which induce the dispersion and electrostatic forces, enhancing CO_2 adsorption and separation abilities on MOFs.[56] For instance, Bae *et al.* reported the adsorption capacity of an amine-functionalized MOF (IRMOF-3 S_{BET} = 2160 m^2 g^{-1}) up to 52.6 mg g^{-1}, this result is surprising if it is compared with its non-functionalized counterpart (MOF-5 S_{BET} = 2833 m^2 g^{-1}) that is able to adsorb 48.2 mg g^{-1} under the same conditions but with a *ca.* 24% increment of specific surface area.[56]

For these very reasons, the design of MOFs decorated with LBSs has grown exponentially given their proven synergy, which leads to improved CO_2 binding affinities, selectivity and CO_2 reversibility. For instance, different MOFs have been functionalized using 2-amino-terephthalic acid (NH_2-H_2BDC) such as NH_2-MIL-53, NH_2-UiO-66, and NH_2-MIL-125 and similar phenomena were observed.[55,57,58] Additionally, other nitrogen-containing linkers, including pyrimidines, triazines, and azoles, have also been tested to synthesize MOFs with LBSs.[59–62]

Finally, to overcome the main limitation exposed in OMSs–MOFs related to water stability, Flaig *et al.* proposed the amino functionalization of several IRMOF-74-III as promising materials to improve the capture of CO_2 in the presence of water.[63] As shown in Fig. 4, Shi *et al.* reported the design of thermally and chemically robust amine-functionalized MOFs formed from triazolate linkers for post-combustion CO_2 capture from flue gas containing water vapour (Fig. 4a). This research reached not only a CO_2/N_2 thermodynamic adsorption selectivity as high as 120 (Fig. 4b and c) but also a CO_2/H_2O kinetic adsorption selectivity up to 70, featuring distinct adsorptive sites at the channel centre for CO_2 and at the corner for H_2O, respectively (Fig. 4d).[64]

3.1.3. Linkers with polar functional groups. The interactions between the functionalized linker and the CO_2 molecule is essential to enhance CO_2 capture. An alternative to the already discussed OMS- and LBS-promoted MOF systems for CO_2 capture is the introduction of polar substituent groups such as –F, –Br, –Cl, –OH, –COOH, –NO_2 and SO_3. Generally, two methods have been employed to synthesise functionalized MOFs with polar functional groups: (i) the direct synthesis using functionalized linkers and (ii) the post-synthesis incorporation of these groups.[28]

An example of the direct synthesis of MOFs with polar functional groups was reported by Barnerjee *et al.*, who synthesised seven different ZIFs with a GME topology (Fig. 5a). ZIF-78 which is a MOF with –NO_2 functional groups adsorbed up to 60 cm^3 cm^{-3} CO_2 at 298 K and 800 torr, which is much higher in comparison with those of the other MOFs from the series (Fig. 5b).[65]

The second strategy, which involves the deviation from the commonplace metal-carboxylate chemistry in MOFs, has

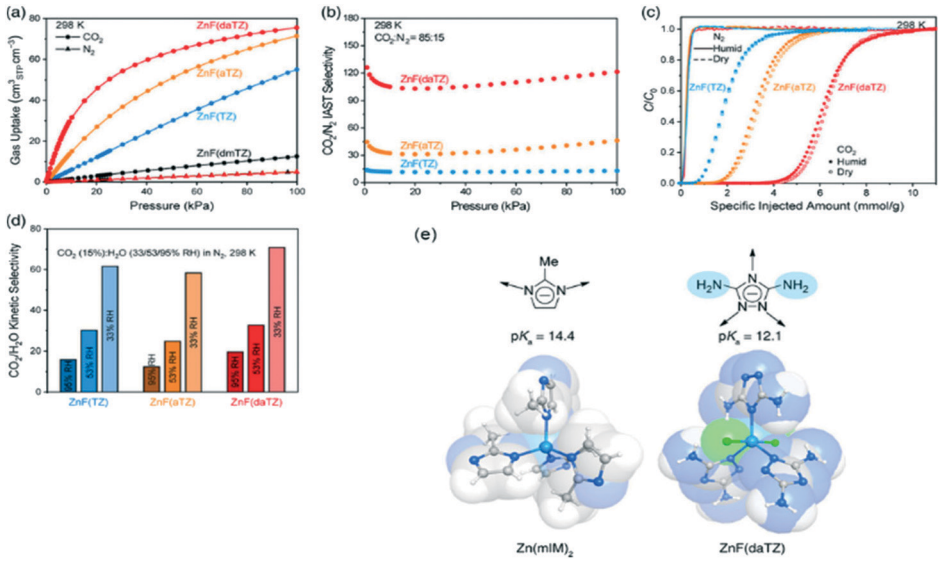

Fig. 4 Evaluation of the metal triazolate frameworks for high-humidity flue gas CO_2 capture. (a) CO_2 and N_2 uptakes at 298 K and 0–1 bar. (b) CO_2/N_2IAST selectivity for the CO_2/N_2 ($v:v$ = 15 : 85) mixed gas at 298 K. (c) Breakthrough curves under dry and humid conditions (~99% RH) for the CO_2/N_2 ($v:v$ = 15 : 85) mixed gas at 298 K and a flow rate of 1 mL min^{-1}. (d) CO_2/H_2O adsorption kinetic selectivities under various relative humidities. (e) Scheme of robust MOFs with azolate linkers (reproduced from ref. 64 with permission from the American Chemical Society, copyright 2021).

triggered the development of structures with a highly polar pore environment. The mixed linker TMOF-1 charged with sulfonated polar groups presented a total uptake capacity of up to 6.8 mmol g^{-1} at 308 K and 1 bar.[66]

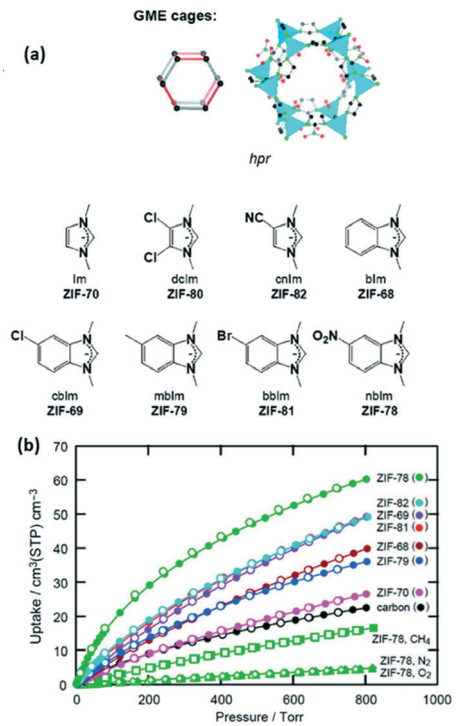

Fig. 5 (a) Scheme of GME cage ZIFs, (b) CO_2 adsorption isotherms at 298 K and 800 torr (reproduced from ref. 65 with permission from the American Chemical Society, copyright 2021).

The designability and flexibility of MOFs with polar functional groups have allowed using these materials for CO_2 capture under different environments such as humid flows or mixed flows which are a more realistic representation of industrial flue gases.[67–69]

3.1.4. MOF flexibility. One of the most studied properties in MOFs is related to the structural reaction to an external stimulus such as gas pressure, temperature, or light.[70,71] Some MOFs exhibit a unique phenomenon called flexibility as a consequence of the interactions and stimuli of molecules on the MOF structure. In order to classify MOFs depending on this intriguing property, MOFs have been grouped as rigid MOFs and flexible MOFs or soft porous crystals.[72] Although the flexibility of MOFs is commonly associated as the result of the framework's external stimulus, it is important to mention that this phenomenon may also be caused by the intrinsic composition of the framework.[73]

As shown in Fig. 6, the external stimuli or the initiator of the flexibility is found to greatly impact the structural change of the framework, such as phase change or change in unit cell parameters. The different flexibility modes in soft MOFs have been classified as breathing phenomena (Fig. 6A), swelling (Fig. 6B), linker rotation (Fig. 6C), and subnetwork displacement (Fig. 6D).

It has been widely reported that certain flexible MOFs exhibit a breathing phenomenon as a consequence of CO_2 adsorption.[72–75] This effect is evidenced in the CO_2 isotherm as a drastic change in the total CO_2 uptake amount at a certain relative pressure. One of the first examples of flexibility in MOFs as a consequence of CO_2 adsorption was reported by Aguado *et al.* in ZIF-7. Fig. 7 shows the CO_2 adsorption isotherm of ZIF-7 at different temperatures and

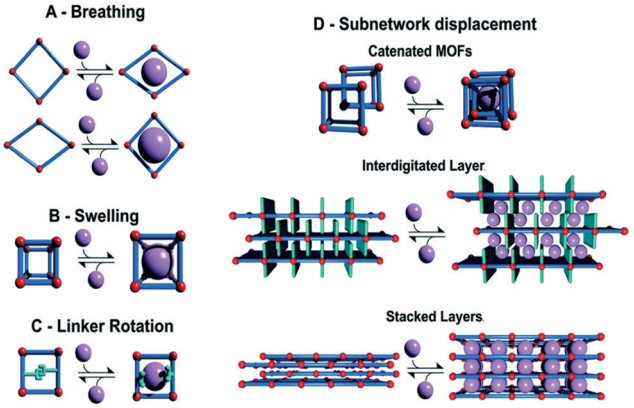

Fig. 6 Classification of different flexibility modes of MOFs. One class is characterized by the change in unit cell volume ($\Delta V \neq 0$; A, B and D) while in the other case the unit cell volume does not change ($\Delta V = 0$; C and D) (reproduced from ref. 73 with permission from the Royal Society of Chemistry, copyright 2021).

200 kPa, where a drastic change in the total CO_2 uptake is observed at a pressure of 50 kPa.[76] *In situ* synchrotron X-ray diffraction experiments have allowed classifying these structural changes in ZIF-7 as different MOF phases.[77,78]

Interpenetrated MOFs have shown to present high structural flexibility to gas molecule adsorption.[79–82] A good example is the breathing of a 2-fold interpenetrated microporous MOF with a flexible tetrahedral organic linker and Zn^{2+} clusters that adsorb CO_2. The CO_2 adsorption isotherm revealed a drastic adsorption step at about 10 bar and a significant hysteresis during CO_2 desorption reaching a total uptake of 7.1 mmol g^{-1} at 30 bar and 298 K.[79]

3.1.5. Pore size control and hydrophobicity. The high versatility of MOFs attached to a wide number of linkers available in the market has allowed designing MOFs with a variety of desirable pore sizes working as molecular sieves. CO_2 has a rather small kinetic diameter (3.3 Å), favouring its adsorption into materials that possess micropores rather than mesopores or macropores. Even though generally MOFs are characterized by the enhancement of CO_2 adsorption uptake *via* linker or metal functionalization, it has also been proved that the design of MOFs with altered linker length offers an improvement in the adsorption of CO_2.[83–86]

The competitive adsorption of water and its impact on the stability of MOFs have been a major concern for practical applications in CO_2 capture. Many MOFs have been demonstrated to undergo structural degradation because the framework presents stronger interactions with the water than the CO_2 due to its quadrupole moment.[87–89] Hydrophobic MOFs, with improved water stability and low affinity toward water, are a class of promising adsorbents for CO_2 capture under humid conditions.[90–94]

ZIFs have been characterized for their hydrophobic behaviour; for instance, Nguyen *et al.* reported the selective CO_2 adsorption properties of hydrophobic ZIF-300, ZIF-301, and ZIF-302. These MOFs showed very low affinities toward water, as confirmed by their low water uptakes (6, 5.8, and 4.5 mg g^{-1} at $P/P_0 \approx 0.8$ and 298 K, respectively) while CO_2 adsorption isotherms at 298 K and 800 torr indicated CO_2 uptakes of 40, 40, and 36 cm^3 cm^{-3}, respectively.[95]

3.2. Post-synthesis MOF modification

The development of strategies to introduce new sites with high affinity to CO_2 into MOFs has been attracting attention recently due to their main approaches of non-altering or damaging the core of the structure.[96] The post-synthesis modification (PSM) in MOFs has managed to enhance the CO_2 affinity through strategies such as the modification of the linker of functional groups, *e.g.* amine groups and polar groups, or not only by exchanging the metal in the secondary building units (SBUs), but also by the modification, insertion or exchange of organic linkers.

In 2009 Bae *et al.* reported the post-synthesis modification of a 3D non-catenated Zn-paddlewheel MOF (Fig. 8) by replacing coordinated solvent molecules with highly polar ligands leading to considerable enhancement of CO_2/N_2 selectivity. This post-synthesis modification allowed improvement of the CO_2 selectivity at low loading over other molecules such as N_2 or CH_4.[97]

The post-synthesis modification as a novel approach to enhance the CO_2 capture in MOFs is not limited to the coordination environment of the metal cluster. Metal exchange in SBUs is also a promising technique that can improve the CO_2 uptake and selectivity. For instance, UiO-66 initially formed from zirconium clusters was modified with

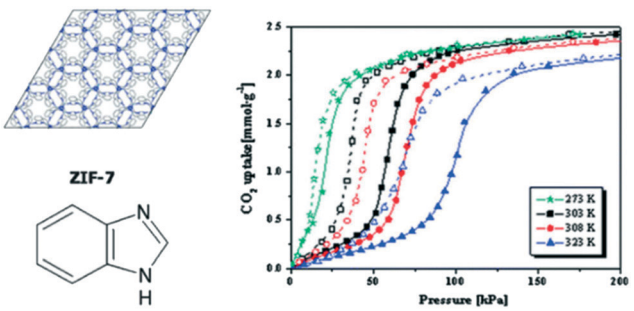

Fig. 7 Schematic structure of ZIF-7 and CO_2 adsorption isotherms for ZIF-7 at several different temperatures at 200 kPa (reproduced from ref. 76 with permission from the Royal Society of Chemistry, copyright 2021).

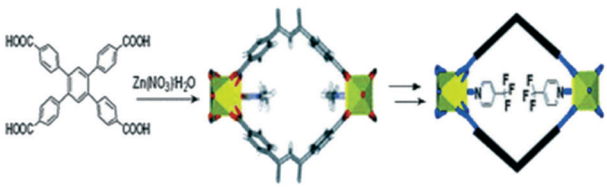

Fig. 8 Scheme of post-synthesis modification of a 3D non-catenated Zn-paddlewheel MOF (reproduced from ref. 97 with permission from the Royal Society of Chemistry, copyright 2021).

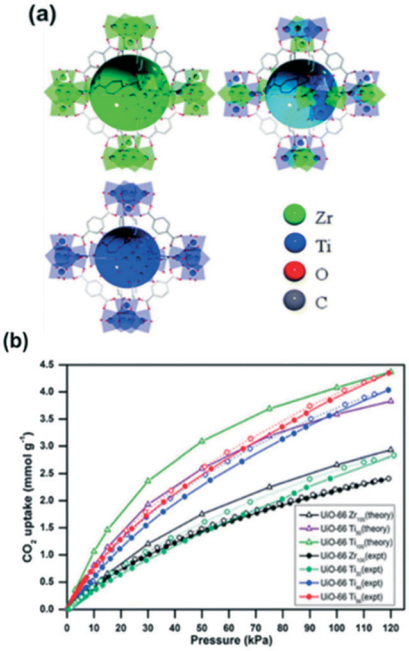

Fig. 9 (a) A schematic representation of UiO-66 (Zr), UiO-66 (Zr,Ti) and UiO-66 (Ti); (b) CO_2 isotherms for UiO-66 Zr and Ti at 273 K and 120 kPa (reproduced from ref. 98 with permission from the Royal Society of Chemistry, copyright 2021).

titanium ions (Fig. 9a) showing a drastic increase in the total CO_2 uptake (Fig. 9b).

The CO_2 uptake in zirconium MOF UiO-66 was observed to be almost double with the post-synthetic exchange of Zr by Ti. This was explained to be due to the smaller pore size and higher adsorption enthalpy. Furthermore, the full effect is obtained with 50% Ti loading, precluding the need to fully substitute frameworks for CO_2 capture.[98]

The post-synthesis exchange in MOFs is not restricted to the change of metal ions in the SBUs. For instance, different approaches have been reported to enhance the CO_2 capture capability *via* linker exchange. Recently, Kronast *et al.* successfully used the PSM to introduce molecular gates into the MOF UiO-66-allyl. The obtained functionalities enable powerful tuning for the adsorption of CO_2 over N_2.[99]

3.3. MOF-based composite materials

The commercialization of MOFs has been limited by their crystalline or microcrystalline form, which inherently limits their integration into many technologies. A big effort has been done to incorporate and create a synergy of different matrices with potential realistic applications.

In terms of CO_2 uptake capacities in MOF composites, they are typically a great deal larger than those of the parent MOFs due to the generation of new pore environment(s), additional interactions at the interface between phases, and/or affinity of CO_2 to the guest(s). Moreover, the plasticity and chemical stability of certain compounds utilized in the formation of MOF composites can lead to enhanced stabilities and mechanical properties of the resultant materials.[16,28]

MOF–polymer composites are a relatively recent addition to the class of MOF composites widely studied for CO_2 capture and separation. They tend to attract a lot of attention owing to not only the variety of possible polymer functionalities as well as their light weight, facile processability and chemical stability but also the selectivity and applicability of MOFs for CO_2 capture and separation.[100] Different approaches have been used to develop elegant methods to synthesize MOF–polymer hybrid materials. Top-down approaches are performed when MOFs are initially synthesized and subsequently incorporated into polymeric materials, contrarily to what is done in bottom-up approaches, where hybrid materials are synthesized in conjunction with MOF formation.[101]

As summarized in Fig. 10, different approaches for MOF–polymer hybrid materials have been explored by research groups through the synthesis of mixed matrix membranes (MMMs), polymers grafted from MOF particles, polymers grafted through MOFs, polymers templating MOF growth and MOFs using polymer ligands.

The most widely used methods to synthesize MOF-based MMMs are the simple solution, dispersion and casting methods.[102–104] For example, Su *et al.* used UiO-66-NH_2 and PSF (polysulfone) to obtain MMMs (50 wt% MOF) with a remarkable selectivity for CO_2 compared to CH_4 and N_2.[105] The differences between MIL-53(Al) and MIL-53(Al)-NH_2 PVDF-based membranes were reported by monitoring their selectivity toward a gas combination of He/CH_4 and CO_2/CH_4 which was preferential to He over CH_4 and CO_2 over CH_4 on the MIL-53(Al)-NH_2 based composite.[106] In the last decade, there is a high number of publications for MOF-based MMMs, such as PVDF/(UiO-66, UiO-66-NH_2, MIL-53, MIL-101, HKUST-1 and ZIF-8) obtaining potential applications for flexible gas separation.[104]

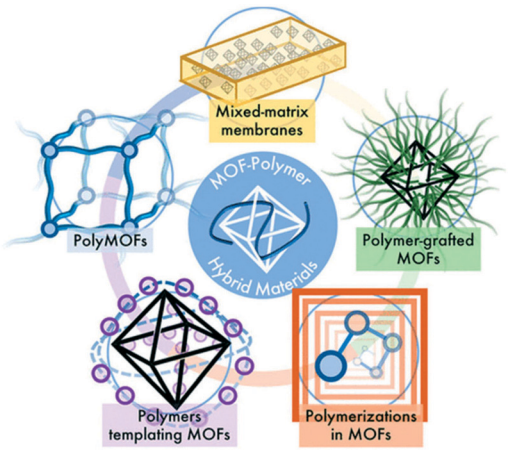

Fig. 10 Overview of synthesis approaches for MOF–polymer hybrid materials (reproduced from ref. 101 with permission from the American Chemical Society, copyright 2021).

3.4. Engineering aspects in CO_2 capture in MOFs

Commonly, the evaluation of gas sorption properties of porous materials such as MOFs mainly relies on single-component gas sorption isotherms and crystallographic techniques, which are able to disclose the microscopic sorption sites and properties of gas molecules. However, studies on the macroscopic and practical mixture gas separation performance of MOFs remain limited. To bridge the gap between materials described in the last section and engineering aspects, we herein summarize the main approaches in the literature for the practical gas separation performance, including adsorption heat, ideal, and real gas selectivity, multicomponent gas adsorption, and cyclic mechanic stability.

3.4.1. Isosteric heat of adsorption. The quantification of the interactions between the adsorbents and adsorbates is a factor of high importance due to their direct relationship to the design of regeneration processes.[107] Generally, the heat of adsorption can be calculated by the Clausius–Clapeyron equation under the considerations that (i) the adsorbed gas follows the characteristics of an ideal gas and (ii) the volume of the gas adsorbed is negligible.[108] The most common way to calculate isosteric heat of adsorption (Q_{st}) is to measure gas sorption isotherms at different temperatures and perform a mathematical fitting using the virial equation (eqn (1) and (2)).[109]

$$\ln P = \ln N + \frac{1}{T}\sum_{i=0}^{m} a_i N^i + \sum_{i=0}^{n} b_i N^i \quad (1)$$

$$Q_{st} = -R\sum_{i=0}^{m} a_i N^i \quad (2)$$

where P is the pressure (bar), N is the adsorbed quantity (mmol g^{-1}), T is the temperature (K), R is the gas constant (8.314 J K^{-1} mol^{-1}), a_i and b_i are the virial coefficients, and m and n represent the number of coefficients required to describe the isotherms adequately.

Several publications explored the use of isosteric heat of adsorption as a parameter to determine the improvement in the adsorbate–adsorbent interaction and its impact on the gas selectivity of structural functionalized MOFs.[110–112] A good example is the one reported by Park *et al.*, which showed enhanced isosteric heat, selectivity, and uptake capacity of CO_2 adsorption on SNU-100 by impregnation of various metal ions such as Li^+, Mg^{2+}, Ca^{2+}, Co^{2+}, and Ni^{2+}.[112] Due to the electrostatic interactions between CO_2 and the extra-framework metal ions, the isosteric heat of CO_2 adsorption was observed to be increased to 37.4–34.5 kJ mol^{-1} and the CO_2 adsorption selectivities over N_2 at room temperature are increased to 40.4–31.0, compared with those (29.3 kJ mol^{-1} and 25.5, respectively) of the parent MOF (SNU-100).

3.4.2. Ideal adsorbed solution theory (IAST). The implementation of CO_2 capture engineering processes requires the study of both single component and more important mixture component adsorption–desorption equilibrium.[113] It is recognized that single component isotherms can be easily obtained more commonly by volumetric adsorption experiments. However, multicomponent adsorption equilibrium studies present a challenge since different variables are involved in the processes.[69,114] IAST has been developed as an alternative to overcome these challenges and limitations under the major considerations that (i) the adsorbed molecules in the material have equal access to the inner pores, (ii) the surface of the material is homogeneous, and most importantly (iii) the intermolecular interactions are equal in strengths, which means that the mixture is an ideal solution.[115,116] This method which describes the multicomponent adsorption isotherms from single-component adsorption isotherms starts from Raoults' law type of relationship between the fluid and adsorbed phase. Using the mathematical fitting explained in detail by Myers & Prausnitz, the IAST allows the selectivity of an ideal multicomponent mixture to be calculated.[115] For a binary mixture, the selectivity can be calculated as represented in eqn (3).

$$S_{ads} = \frac{q_1/q_2}{p_1/p_2} \quad (3)$$

IAST has been widely applied in MOFs to study the selectivities for separation of mixtures of industrial interest such as N_2/CO_2, CH_4/CO_2 or CH_4/N_2.[56,117–119] Billemont *et al.* use the IAST to study experimentally and theoretically the multicomponent co-adsorption of captured CO_2, biogas and purified natural gas in MIL-100 (Fe) MOF. IAST showed to be a suitable model for such applications and seems appropriate for CO_2/N_2 separation in MIL-100 (Fe). Due to the versatility in terms of ligands and metals in MOFs, any adsorption application must be considered carefully, and IAST predictions should be supported by previous experimental validation.[114]

3.4.3. Dynamic column breakthrough experiments and their application in multi-component CO_2 capture capacity. The understanding of the equilibrium adsorption in processed mixed gas is essential for the screening of the best adsorbent material, the design of the process, and the validation of theoretical models of mixture adsorption.[120] Generally speaking, breakthrough experiments allow measurement of gas mixture equilibrium and evaluation of the capability of the adsorbent material to fulfil adsorption aims. The breakthrough theory for mixed gas equilibrium whose basis is the mass balance across the whole packed column (in − out = accumulation) has been widely described by different authors in the literature.[121–124]

In a common breakthrough experiment, a volumetric or gravimetric apparatus is coupled with a gas chromatograph or mass spectrometer in order to measure the co-adsorption isotherms of CO_2 and other gases.[69,114,125] Due to the lack of commercial equipment for breakthrough experiments, many of these tests are carried out using in-house designed setups.

However, the accuracy and the operational control can vary and by consequence, lead to experimental errors.

This engineering approach can be applied to evaluate MOF adsorbents in terms of multi-component adsorption performance and show a screen between ideal and practical adsorption at an industrial level. Even though MOFs can show a remarkable adsorption uptake for single-component adsorption, these materials do not necessarily perform well in binary or multi-component gas mixtures. To evaluate the co-adsorption performance of CO_2 under real conditions, dynamic column breakthrough experiments are carried out.[69,126] Xiang *et al.* reported the binary co-adsorption of CO_2/N_2 and CH_4/CO_2 in several different MOFs. In this publication, Mg-MOF-74 which is characterized by having open metal sites that enhance the CO_2 capture in single-component adsorption experiments showed that under dynamic binary adsorption conditions (N_2/CO_2), it is able to adsorb up to 5.87 mmol g^{-1} at 298 K, which is less than half the total uptake amount reported for single-component adsorption capacity.[127,128] Hu *et al.* reported the design of a lab-scale high accuracy device (Fig. 11) for the co-adsorption of CO_2 into a highly stable MOF (UiO-66–OH) with an optimum aperture size (3.93 Å). They described the details of appropriate procedures for performing breakthrough experiments taking into account unavoidable pressure drop and changing the exit flow rate. In addition, they provided a complete analysis of breakthrough responses and demonstrated their application in a complete evaluation of MOF materials for post-combustion CO_2 capture.[129]

From a practical point of view, the evaluation of MOFs in CO_2 co-adsorption in a binary mixture is not enough since real flue gas usually contains other molecules such as water (5–15%) or N_2 which have a great influence on the CO_2 adsorption performance.[130–132] The assessment of the CO_2 capture performance of MOFs in the presence of water vapour is indispensable and ternary $CO_2/N_2/H_2O$ breakthrough tests are needed.[133] Most MOF adsorbents exhibit a decrease in the CO_2 uptake capacities under wet conditions due to the competitive adsorption of H_2O over CO_2, especially for MOFs with vacant Lewis acid sites.[134] For example, Mg-MOF-74 experiences an 83% decrease in CO_2 uptake capacity under wet conditions from 5.87 to 1 mmol g^{-1}.[45,127]

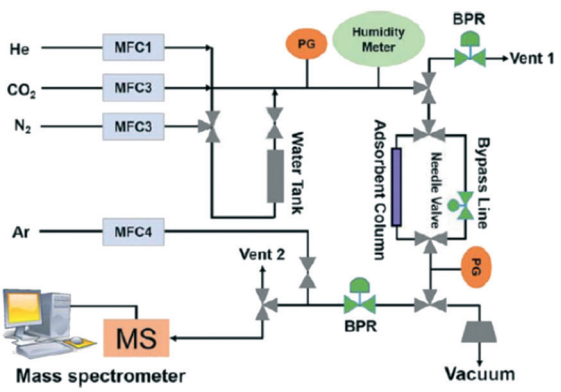

Fig. 11 Breakthrough set-up for CO_2 co-adsorption study (reproduced from ref. 129 with permission from John Wiley and Sons, copyright 2021).

As discussed in the previous section, many efforts have been gathered to improve water stability in MOFs, mainly *via* amine functionalization and enhancing the structural hydrophobicity.[135–137]

3.4.4. Gas diffusivity. Gas diffusivity is one of the most important parameters for gas adsorption concerns in MOFs due to its direct relationship with the mass transfer coefficient which relates the mass transfer rate in separation processes and establishes the specified requirements in the design and manufacture of separation process equipment.[126,138] From a microscopic approach, gas diffusivity can be quantified by the track of the movement of gas molecules or directly trace the concentration profiles of gas molecules within MOF single crystals such as pulsed-field gradient nuclear magnetic resonance (PFG-NMR).[139] From a macroscopic point of view, gas diffusivity can be estimated on the basis of the overall gas adsorption behaviour of MOF powders.[140] The main estimations are through batch adsorption, frequency response or breakthrough experiments.[141–144]

Tanaka *et al.* reported a systematic study of tuning the size of ZIF-8 crystals and investigated the size dependence of *n*-butanol diffusion inside ZIF-8 crystals.[145] By fitting the fractional uptake curve with mathematical models, they found that gas diffusion inside large crystals (>88 μm) is well monitored by a micropore diffusion model, while the surface resistance model is more suitable for smaller crystals. This result suggests that downsizing the crystal may lead to increased surface resistance.

The frequency response (FR) for gas diffusion measurements has been used as a tool to estimate gas diffusivity. In a typical frequency response experiment, one of the adsorption parameters (*e.g.* volume, flow rate, concentration, or pressure) is perturbed sinusoidally, and as a consequence, the other parameters react periodically but with different phase lag and amplitudes.[146] These responses allow calculating the gas diffusivity in porous materials.[134] Recently, concentration swing FR (CSFR) has been applied to study CO_2 diffusion in large Cu–BTC single crystals, revealing a micropore diffusion coefficient of 1.7×10^{-9} m^2 s^{-1} with negligible dependence on CO_2 concentration from 0.1 to 10%.[147]

3.4.5. MOF process, cycles and regeneration. Naturally, adsorbent materials do not possess infinite CO_2 uptake capacity. Therefore, continuous interaction with flue gas or atmospheric mixtures will eventually lead to a thermodynamic equilibrium between the solid and gas phases, where the rates of adsorption and desorption are equal.[126] A further flow of feed gas mixtures will make this technology less effective. Under this premise, it is of high importance to regenerate the adsorbents and design semi-continuous processes in which the adsorption and adsorptive regeneration processes can be combined.

The process design is a fundamental step in order to potentiate the application of porous materials. Adsorbents are commonly supported by fine metal meshes in a fixed bed, or quartz wool if the material is in powder form. For MOFs, most of them are prepared in powder form and thus need to be pelletized before being secured in a fixed bed. In this way, the cross-column pressure drop can also be minimized to enhance the column breakthrough dynamics.[129]

MOF-based monoliths have appeared as an improved approach to potentiate the CO_2 adsorption uptake.[148,149] Connolly *et al.* reported the synthesis of metal–organic gel (MOG)-based macroscopic monoliths of UiO-66 with extraordinary properties to capture CO_2 reaching a total uptake capacity of up to 0.67 g g^{-1} CO_2 at 298 K and 40 bar.[149] A similar strategy was performed by Lawson *et al.* to carry out gas stream purification at CO_2 low pressure by the incorporation of tetraethylenepentamine in a novel post-synthesis monolith synthesis (Fig. 12).[150]

Glass MOF materials have been reported recently as a novel strategy to develop MOF monoliths through the development of MOF crystal–glass and MOF blended composites. MOF glasses are formed by a melt-quenching process which results in structural amorphization. For instance, Bennett's group has widely explored different approaches to form glass MOF-based composites such as porous MOF–glass, MOF crystal–glass, flux melted glass and blended ZIF—glass composites.[151]

At an industrial scale, the adsorption step is generally followed by another one to make a cyclic adsorption process which sometimes is carried out in a continuous manner if the adsorbent has a low price or the regeneration processes are complicated.[152] In most processes, the regeneration of the adsorbent is essential since the disposal of the material as waste is not economical. In practice, the regeneration is performed by different routes, either *in situ* or externally by procedures such as an increase in the temperature, reduction in the partial pressure of the adsorbates, reduction in the concentration or inert gas purging.[134] For the regeneration of MOFs, it is necessary to compare their respective heat of CO_2 adsorption *versus* binary adsorption capacity since it is highly related to not only their cycling and regeneration processes but also their structural stability and chemistry surface.[153]

3.4.6. Cost of the MOFs. MOFs are a relatively new family of porous materials which, due to their nature being formed from organic linkers and metal clusters, have been obtained through expensive reactants (organic solvents, organic linkers and metal salts) and energy-consuming procedures (high temperature synthesis and purification procedures). The cost of MOFs is their main limiting factor for commercialization and industrial applications. A big research effort has been made to optimize synthesis methods but most importantly to use economically appealing starting materials. However, the selling price of MOFs from commercial suppliers is still much higher than those of most of the conventional adsorbents such as activated carbon. Herein the MOF research community still has room for further research to significantly decrease manufacturing cost and make MOFs the technology of choice for gas adsorption.

3.5. Mechanistic insights and *operando* studies for CO_2 capture in MOFs

The interpretation of the CO_2 capture efficiency based on *ex situ* characterization methods may be sometimes misleading. For understanding and further designing more efficient molecular organic framework (MOF) materials, it is required to clearly establish an intrinsic structure–property relationship, which describes the location of adsorption sites on the atomic-scale surface structure inside the pores and the identification of beneficial interactions for the adsorption of CO_2. Therefore, visualization of the guest–host interactions involved in the gas sorption process is crucial to shed light on how these materials operate under working conditions and to elucidate potential mechanisms for the selective CO_2 capture.

From this perspective, the application of advanced characterization techniques with high spatial and time resolution under operation conditions is required to examine the porous frameworks during the gas sorption process. As shown in Fig. 13, the development of *in situ* and/or *operando* methods are gaining growing interest for monitoring the structural dynamic features, identifying the preferable CO_2 binding sites and understanding the mechanism of CO_2

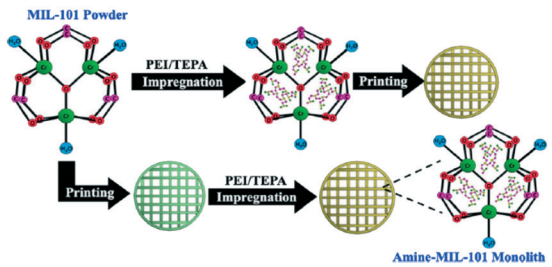

Fig. 12 Formation process of amine-MIL-100 monoliths (reproduced from ref. 150 with permission from the American Chemical Society, copyright 2021).

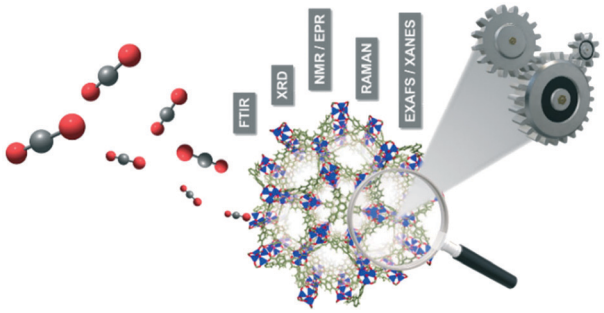

Fig. 13 Representative illustration of the *operando*/*in situ* characterization approach applied to framework porous materials during the CO_2 gas sorption process.

adsorption. At this point, they must be distinguished from either *in situ* or *operando* terms. While *in situ* methods are referred to as the adsorption/desorption of specific probe molecules under controlled environment and temperature conditions, *operando* approaches allow one to directly correlate the structure, porosity and composition of framework porous materials to their performance under realistic operating conditions.[154–157] A perfect *operando* experiment would correlate the nanoscale structure with the bulk scale performance considering the spatiotemporal heterogeneities.[158] Therefore, any *operando* study requires in depth-understanding of local chemical and physical properties (molecular surface species and temperature/heat/mass transport gradients) under working environment conditions and besides has the capability to analyze these properties in real time with high spatiotemporal resolution.

In general, multiple *in situ*/*operando* characterization techniques have been applied to the study of CO_2 capture in framework porous materials. Diverse examples can be found based on spectroscopic methods such as Raman and infrared (IR) spectroscopy, nuclear magnetic resonance (NMR) and electron paramagnetic resonance (EPR).[159–161] These methods provide detailed information on the frameworks and on the host–guest interactions revealing the nature of these binding interactions. On the other hand, synchrotron characterization-based techniques are also widely used for the characterization of MOFs. These techniques essentially include extended X-ray absorption fine structure (EXAFS), X-ray absorption near-edge structure (XANES) and *in situ* diffraction/scattering experiments, which are typically used to determine the crystallographic sites preferred for CO_2 capture inside the pores as well as their coordinative environment as a function of gas loading.[162–164] In this section, we overview several examples representative of the most significant advances in the application of *in situ*/*operando* characterization techniques to elucidate the gas sorption mechanism in CO_2 capture on porous framework materials.

Recently, Hadjiivanov *et al.* have reported an interesting review in which all the varieties of functionalities and porous structures of framework porous materials are described as well as the mechanisms of interaction with guest molecules measured by vibrational spectroscopy.[160] Depending on the type of MOF, IR spectroscopy data indicate that carbon dioxide can be physically adsorbed on three types of centres: (i) coordinatively unsaturated metal cations, (ii) hydroxyl groups, and (iii) organic linker sites such as aromatic rings, carboxylate groups or C=C and C–C inter-ring bonds, among others. Furthermore, the adsorbed CO_2 over MOFs functionalized with amines or amides undergoes CO_2 chemical transformation. Couck *et al.* evidenced by *in situ* DRIFTS (diffuse-reflectance infrared spectroscopy) that this strong interaction is due to the formation of electron donor–acceptor (EDA) complexes between CO_2, the amino group and the hydroxyl group of the framework structure.[55] Meanwhile, the formation of this type of EDA complex is also possible in the absence of amines as suggested in the work reported by Llewellyn *et al.*[165] *Operando* IR spectroscopy was used to discriminate the type of CO_2 interaction in MIL-101 (Cr), MIL-53 (Cr) and MIL-47 (V). CO_2 is linearly coordinated on the Lewis acid coordinatively unsaturated Cr^{3+} sites of MIL-101 (Cr), while the carbon atom of CO_2 interacts with the oxygen of the Cr–OH group forming an electron donor–acceptor complex on MIL-53 (V). In contrast, neither of these types of interactions are observed on MIL-47 (V), and CO_2 pseudo-liquid-like species are formed inside the pores in the absence of any specific adsorption site.

Nuclear magnetic resonance (NMR) and electronic paramagnetic resonance (EPR) spectroscopy techniques provide detailed information at the molecular level on the local chemical environment, including molecular motion in metal–organic frameworks. Lu *et al.* performed an interesting study based on computational molecular dynamics and *in situ* solid-state NMR measurements to elucidate the CO_2 adsorption mechanism on an α-magnesium formate MOF.[166] They observed that CO_2 motion is restricted at high temperatures and demonstrated that the CO_2 guest interacts efficiently with the hydrogen atoms of the formate linker oriented toward the interior of the MOF pores. It should be mentioned that NMR spectroscopy is also a powerful tool to study the diffusion of guest molecules within the pores and channels of porous framework materials.[162] The knowledge of the kinetics gas loading is crucial to optimize gas sorption processes on an industrial scale.

In contrast to NMR spectroscopy, EPR deals with the interaction of electromagnetic radiation with inherent magnetic moments associated with unpaired electron spins present in paramagnetic species such as transition metals (*e.g.* Ti^{3+}, Mn^{2+}, Cu^{2+}, Cr^{3+}or Co^{2+}) or inorganic/organic free radicals. EPR spectroscopy provides unique information about the nature, coordination environment, symmetry and electronic ground state of paramagnetic species in framework porous materials.[159] EPR is a very sensitive technique and is capable of analyzing the local geometry of paramagnetic metal ions even in small concentrations randomly distributed over a diamagnetic parent framework.[167] By means of *in situ* EPR measurements, Mendt *et al.* investigated the breathing behaviour during the CO_2 sorption process on the flexible and pillared-layered MOF $Zn_{1.9}Cu_{0.1}$(BME-bdc)$_2$(dabco).[168] The monometallic MOF $Zn_{1.9}$(BME-bdc)$_2$(dabco) parent exhibits a reversible transition from a narrow pore phase to an expanded open pore upon guest inclusion. The doping with paramagnetic Cu^{2+} ions as probe molecules allowed this phase transition to be monitored on a microscopic scale using EPR spectroscopy. This technique is highly sensitive to small structural changes in the Cu^{2+} coordination induced by CO_2 interaction, and the results obtained showed a remarkable breathing behavior with a cell volume increase of 20% for the large pore phase.

X-ray absorption spectroscopy (XAS) and high-resolution X-ray diffraction (HR-XRD) measurements using radiation synchrotron sources are very useful approaches to analyze the local atomic structure related to the geometry, coordination

and interatomic distances as well as the positions of adsorbed guests in the pores. The comprehensive review reported by Soldatov *et al.* overviewed the potential of X-ray absorption spectroscopy for the *in situ* characterization of MOFs.[164] In an interesting study, Du *et al.* investigated the CO_2 adsorption mechanism on three commercial MOFs (Cu–BTC, Fe–BTC and ZIF-8) by using XANES analysis and EXAFS fittings.[169] They found that the oxidation states, bond distances and coordination numbers of the first shell remain unaltered in the three solids during the adsorption/desorption of CO_2 suggesting that physical adsorption is the main driving force in the CO_2 capture by the three framework porous materials. This observation reveals that CO_2 capture in MOFs is energetically much more efficient than capture by chemical adsorbents based on amines because physical adsorption requires less energy for regeneration.

On the other hand, Giacobbe *et al.* reported an exhaustive study to disclose the adsorption sites occupied by the CO_2 gaseous probe and the nature of host–guest interactions on the metal–organic framework $Fe_2(BPEB)_3$ as a CO_2 adsorbent by means of *in situ*/*operando* high-resolution and high-energy X-ray diffraction measurements at several pressures and 298 K.[170] This study provides structural details during CO_2 adsorption on a rigid MOF with remarkable CO_2 adsorption capacity in the absence of framework breathing, phase transition, exposed metal sites or functional groups with high CO_2 specific affinity on the skeleton of ligands. The MOF $Fe_2(BPEB)_3$ presents a structure formed from 1D triangular channels (Fig. 14(a)) in which three types of adsorption sites (CO_2-1, CO_2-2 and CO_2-3) were proposed as shown in Fig. 14(b). The pair distribution function (PDF) analysis presented in Fig. 14(c) and (d) shows the distribution of interatomic distances as a function of CO_2 loading on $Fe_2(BPEB)_3$. These functions are typical of disordered or poorly crystalline materials like $Fe_2(BPEB)_3$, and the peak emerging at 3.2 Å suggests the occurrence of new cooperative guest–host and guest–guest binding interactions with increasing CO_2 loading. Based on these observations, the authors demonstrated that CO_2 molecules interact with the carbon atoms of the triple bond and of the penta- and hexa-atomic rings of the $BPEB^{2-}$ linkers, and these results were supported with molecular dynamics simulations. This work represents a clear example of the potential application of *in situ*/*operando* high-resolution X-ray diffraction analyses to gain structural insight during gas sorption on framework porous solids.

In conclusion, we can highlight that the application of *in situ*/*operando* methods provides new insights into the CO_2 adsorption process. These methods allow locating the adsorption sites inside the pores and the identification of the host–guest binding interactions beneficial for the adsorption of a specific guest, ultimately helping to design rationally more efficient porous framework materials for CO_2 capture and its subsequent utilization.

4. MOFs as advanced catalysts for gas-phase CO_2 conversion

C1 chemistry and catalysis, especially referred to as carbon dioxide (CO_2) transformation, is vital for clean fuel and chemical production to facilitate the transition towards sustainable societies. Burning biomass, organic waste and fossil fuels generates a huge amount of CO_2 emissions, which leads to adverse climate change and drives the scientific community to focus their attention and efforts on CO_2 conversion, especially on the transformation of CO_2 into valuable products.[171–175]

Presently, the CO_2 capture and storage (CCS) technology is considered to be the most effective way to curb CO_2 pollution on a large scale. Nevertheless, most of the current CCS

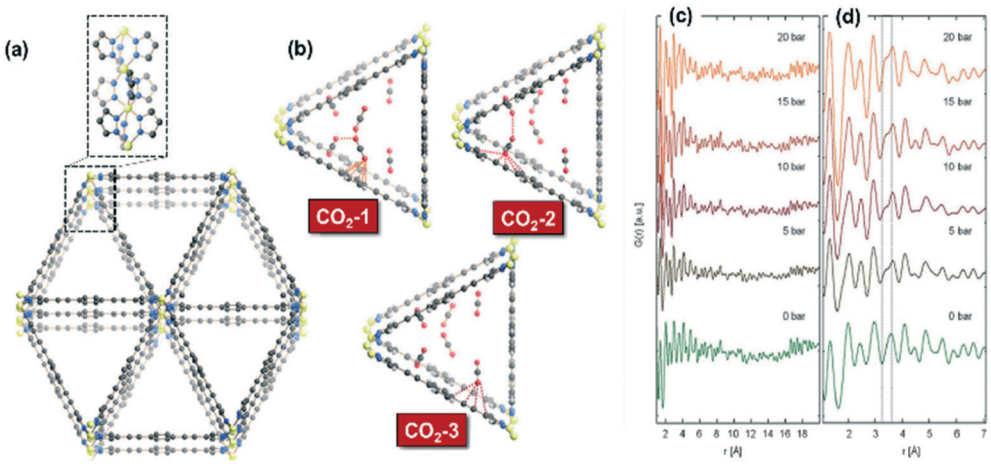

Fig. 14 (a) Crystal structure of $Fe_2(BPEB)_3$ and portion of the 1D metal chain exposed along the *a*-axis; (b) representation in perspective along the [100] direction of host–guest and guest–guest interactions involving the three independent CO_2 adsorption sites at 10 bar and 298 K in $Fe_2(BPEB)_3$; (c) pair distribution functions (PDFs) of $Fe_2(BPEB)_3$ at different CO_2 loadings; (d) magnification in the 1–8 Å range. Atoms: carbon, grey; hydrogen, light grey; iron, yellow; nitrogen, blue; oxygen, red (reproduced from ref. 170 with permission from the Royal Society of Chemistry, copyright 2021).

approaches are deemed highly energy-intensive resulting in elevated cost and limiting their implementation in industrial practice. Hence CO_2 capture and utilisation (CCU) are emerging as an alternative or a complementary strategy to CCS to mitigate CO_2 emissions. Among the multiple CO_2 conversion alternatives, chemical CO_2 recycling in the gas phase constitutes a straightforward approach for effective CO_2 conversion to value-added products like syngas or synthetic methane. In this scenario, some traditional processes such as the dry reforming of methane, the CO_2 methanation and the reverse water gas shift have gained renewed interest from the CO_2 utilisation perspective.[176–179] Indeed, these reactions represent flexible routes to upgrade CO_2, and their application at an industrial scale could substantially reduce CO_2 emissions. Nevertheless, the relatively inert nature and low reactivity of carbon dioxide pose formidable challenges to successfully accomplish these reactions. In particular, the design of highly effective, stable and selective catalysts able to operate under realistic flue gas conditions remains an open quest for the catalysis and reaction engineering community.

In this context, metal–organic frameworks (MOFs), as a relatively new emerging family of crystalline porous materials, have demonstrated promising features as heterogeneous catalysts or supports/precursors to overcome the CO_2 conversion challenge.[180] These materials, also known as porous coordination polymers (PCPs), have unique features and advantages, such as adjustable framework structures, defined and diverse crystal structures (especially confined microenvironment), hybrid composition, *etc.*,[181–183] which enable their excellent performance in various applications including their use as heterogeneous catalysts.

In this section, recent advances in MOFs and MOF-based heterogeneous catalysts for CO_2 chemical conversions, including CO_2 hydrogenation to methane (methanation reaction), CO_2 hydrogenation to CO (reverse water–gas shift reaction) and dry reforming of methane, are reviewed. Overall, we will outline key aspects such as the catalytic performance, catalyst design and advantages of MOFs for CO_2 conversion in line with the spirit of this special issue.

4.1. CO_2 methanation

In recent years, the CO_2 methanation reaction has gained renewed interest because of its role fundamental for implanting the power-to-gas (PWG) technologies in future energy systems, in which captured CO_2 can be transformed into utilizable methane using renewable hydrogen.[184] One of the most fascinating applications of the methanation reaction is the possibility of transforming the Martian carbon dioxide atmosphere into methane and water for fuel production facilitating long-term space exploration missions by space agencies such as NASA.[185]

CO_2 methanation was first studied by Paul Sabatier and Jean-Baptiste Senderens at the beginning of the twentieth century.[186] This reaction is a highly exothermic (ΔH_{298K} = −165 kJ mol^{-1}) and thermodynamically favourable (ΔG_{298K} = −131 kJ mol^{-1}) process that, in the light of Le Chatelier's principle, proceeds at moderate pressures and low temperatures according to the following stoichiometric reaction (4):

$$CO_2(g) + 4H_2(g) \rightarrow CH_4(g) + 2H_2O(g) \quad (4)$$

Due to the exothermic character of the reaction, it presents apparent kinetic limitations and requires an optimal catalyst to achieve a satisfactory reaction rate and methane selectivity.[187] According to the most recent state of the art, several reviews have been reported discussing the successful development of heterogeneous catalysts and the mechanistic relevant aspects of CO_2 methanation.[188–192] So far, the most efficient systems proposed for CO_2 methanation are based on Ni and/or Ru metal-supported catalysts.[193] Other metals such as Fe, Co, Rh, Pt, Pd or Au have also been tested for CO_2 methanation, although these metals are generally less active and/or selective.[194] From the industrial viewpoint, Ni-based catalysts have gained major interest due to their affordable price. Nevertheless, Ni sintering and coke accumulation become important limitations, and new directions on the catalyst design are addressed.

From this perspective, MOFs and their derivative single-site catalysts have been recently reported as robust and promising catalysts for low-temperature CO_2 methanation. However, the development of MOF-based catalysts for CO_2 methanation is still in its infancy and the most relevant papers have been published in the last four years. It is well known that CO_2 hydrogenation is a structure-sensitive reaction, namely the activity and selectivity depend on the metal particle sizes and the exposed facets.[195] In this sense, the utilization of MOFs as precursors for obtaining highly-dispersed metal active sites and single/dual-atom and cluster catalysts has emerged as a very interesting alternative for synthesizing highly stable, selective and active catalysts for CO_2 methanation.[196–200]

One of the pioneering studies using the MOF templating strategy for preparing highly active catalysts in CO_2 methanation was reported by Lippi *et al.*[201] These authors synthesized a Ru/ZrO_2 catalyst derived from a Ru-impregnated UiO-66 MOF and achieved CO_2 conversions in the 96–98% range with high selectivity to methane for more than 160 h of testing at 350 °C and 5 bar. In the same line, Zeng *et al.*[202] prepared a highly dispersed Ni catalyst supported on porous hydrous zirconia derived from the metal–organic framework precursor UiO-66 treated with a strong base. Ni^{2+} sites were incorporated by adsorption onto the hydroxyl-rich hydrous zirconia and subsequently converted into highly dispersed metallic Ni sites for CO_2 methanation, as shown in Fig. 15. The final catalyst showed good activity (TOF of 345 h^{-1}) and stability (4% decrease in activity after 100 h) with a CH_4 selectivity of more than 99% at 350 °C and 40 bar. In another study, Jiang *et al.* also used the UiO-66 MOF directly as a support for highly and

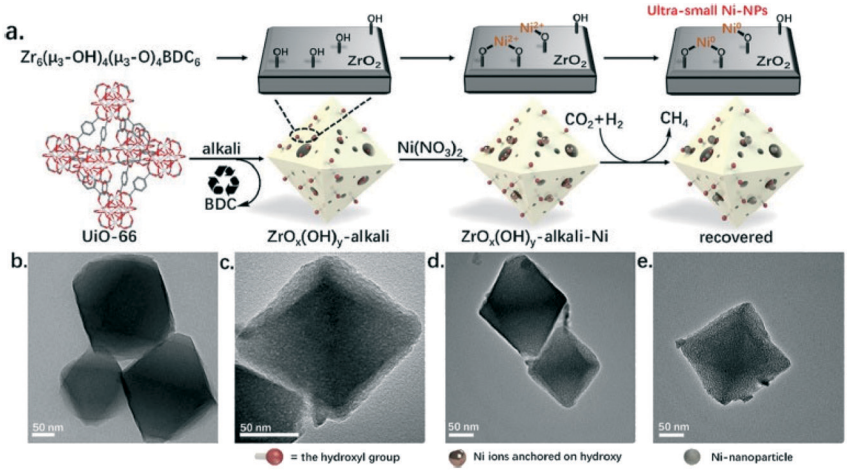

Fig. 15 (a) Schematic representation of the steps followed for the preparation of a highly dispersed Ni catalyst supported on hydrous zirconia derived from the UiO-66 MOF precursor treated with a strong base, and their corresponding TEM micrographs (b–e) (reproduced from ref. 202 with permission from the American Chemical Society, copyright 2021).

uniformly dispersed palladium nanoparticles.[203] These catalysts showed a high activity in CO_2 methanation, and the optimal performance was achieved at 340 °C and 40 bar with a CO_2 conversion of 56%, a CH_4 selectivity of 97.3% and a space–time yield (STY) of 856 g h^{-1} kg_{cat}^{-1}.

Other examples highlight the opportunity of using MOFs as host matrices to confine and stabilize metal single atoms, clusters or nanoparticles. For instance, Zhao *et al.* reported the utilization of the UiO-66 MOF to encapsulate ultrasmall Ni nanoparticles (NPs) with particle sizes ranging from 1.6 to 2.6 nm.[204] In this system, the Ni NPs were highly uniformly dispersed and well isolated by the UiO-66 frameworks, thus avoiding metal sintering effectively. Compared with other traditional supports such as SiO_2 and ZrO_2, Ni@UiO-66 catalysts showed a significantly enhanced catalytic performance for CO_2 methanation in terms of CO_2 conversion (57.6%), selectivity (close to 100%) and long-term stability (100 h) at 300 °C. The highly dispersed Ni NPs decrease the activation energy and facilitate the CO_2 activation. In a similar form, Zhen *et al.* developed an efficient catalyst for CO_2 methanation based on Ni NPs confined in a highly ordered porous MIL-101 framework.[205] These authors demonstrated that in this conformation the Ni (100) facets of the nanoparticles are more exposed and by means of DFT calculations it was estimated that the Ni (100) planes decrease the potential energy barrier for CO_2 dissociation.

Framework porous materials have been extensively used for preparing MOF-derived porous metal@carbon (M@C) composites with specific metal NPs confined in carbon shells with high dispersion. Recently, Prinz *et al.* designed a well-dispersed nickel metal catalyst from thermal decomposition of a Ni-MOF precursor and evaluated the structure–activity relationship during CO_2 methanation using *in situ* X-ray absorption spectroscopy (XAS) and pair distribution function (PDF) analysis.[206] The study reveals that controlling the atmosphere and temperature of thermal decomposition of the Ni-MOF precursor can obtain a Ni@C catalyst in which a carbon matrix of high specific surface area embedded small particles of Ni resulting in a very stable catalyst with high dispersion of active Ni_{fcc} sites. Li *et al.* also reported an interesting study in which a Co-based zeolitic imidazolate framework (ZIF-67) was utilized as a precursor to obtain cobalt nanoparticles inside a carbon matrix in the range from 7 to 20 nm with high resistance to metal sintering.[207] The crystal size and morphology of ZIF-67 were controlled by adding different loadings of cetyltrimethylammonium bromide (CTAB) as a surfactant in the original solution during the preparation. The results obtained suggest that after carbonization, the sample kept the size and morphology

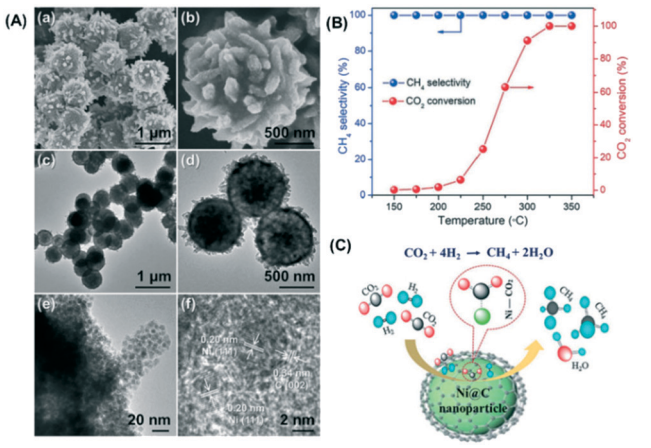

Fig. 16 (A) FESEM micrographs (a and b), TEM images (c–e), and HR-TEM image (f) of the hierarchical Ni@C hollow nanospheres; (B) CO_2 methanation performance of the Ni@C catalyst at different reaction temperatures; (C) schematic representation of CO_2 methanation over the Ni@C catalyst (reproduced from ref. 208 with permission from the Royal Society of Chemistry, copyright 2021).

of the original ZIF-67 crystal with a distorted surface. The optimal amount of CTAB to obtain a carbonized sample with the highest BET surface area and micropore volume was 0.01 wt%, and this catalyst exhibited the highest CO_2 adsorption capacity, CO_2 conversion (52.5%) and CH_4 selectivity (99.2%) at 270 °C and 72 L g^{-1} h^{-1} gas hourly space velocity. In another study, Lin *et al.* prepared hierarchical Ni@C nanospheres composed of dispersed Ni nanoparticles encapsulated by carbon layers, as shown in the images obtained by FESEM and TEM (Fig. 16(A)).[208] The catalytic activity data presented in Fig. 16(B) show that this Ni@C hybrid is an efficient catalyst for CO_2 methanation at atmospheric pressure achieving a CO_2 conversion of 60% and a CH_4 selectivity of almost 100% at 250 °C and 1 bar. From the mechanistic point of view, the authors proposed that CO_2 is activated by electron transfer from the rich d-electrons of metallic Ni NPs to the lowest unoccupied molecular orbital (LUMO) of CO_2 molecules. The reaction proceeds through H_2 dissociation and formation of Ni–C–$(OH)_2$ intermediates that subsequently are hydrogenated to water and methane as products as shown in Fig. 16(C).

Based on fundamental understanding, single-atom based catalysts and confined nanoparticles are an excellent choice to elucidate the mechanism of CO_2 methanation or other energy-related processes at the atomic level. The design of single-atom and metal clusters from metal–organic frameworks presents an ideal platform to investigate the structure–activity relationships with the help of *in situ* characterization methods and theoretical calculation approaches. As Hou *et al.* remarked in their recently published review,[197] although the development and knowledge of single/dual-atom and nanoparticle confined catalysts derived from MOFs are still in the early stages, these systems will be crucial to gain in-depth information at the nanoscopic scale and to design more robust, efficient and economic catalysts achieving the connection between heterogeneous and homogeneous catalyses.

4.2. RWGS

Catalytic conversion of CO_2 to CO by the reverse water–gas shift (RWGS) reaction ($CO_2 + H_2 \leftrightarrow CO + H_2O$) has been largely considered as one of the most prospective application processes for CO_2 hydrogenation. CO_2 conversion *via* the RWGS reaction not only permits high CO_2 conversion efficiency but also facilitates CO_2 reduction to CO, a more valuable chemical which can be used as a raw material in a downstream process such as the FTS reaction or methanol synthesis to produce other high value-added fuels and chemicals.[209]

However, the RWGS reaction is an endothermic reaction, favoured thermodynamically and kinetically at high temperatures resulting in a remarkable energy-demanding process. Consequently, common catalysts often used are easily deactivated by sintering or carbon deposition at these temperatures, hindering the large-scale application of the CO_2 conversion *via* the RWGS reaction.

Currently, research on the RWGS reaction mainly focuses on the study of noble metal catalysts,[210–212] and in more limited extension transition metal catalysts are considered.[213,214] Due to the great significance of the RWGS reaction in both fundamental research and practical applications, the design of low-temperature and high activity RWGS materials has also attracted significant attention recently.[214] Indeed, if the RWGS reactor is conceived to be coupled with a downstream upgrading reactor such as an FTS or MeOH synthesis reactor, the temperature and pressure gaps among both units must be overcome. Hence a medium–low temperature RWGS catalyst is deemed crucial to complete the "CO_2 to fuel/chemical" cycle.[213]

On the other hand, monodispersed supported metal nanoparticles (NPs) have been extensively reported to exhibit catalytic activity in the production of industrially viable chemicals using CO_2 as a carbon pool as discussed in the CO_2 methanation section. Nevertheless, the catalytic activity of metal nanoparticles is limited by their small size, surface quantum, and macro-quantum tunnel effects,[215] and a major barrier to their widespread use is the potential for sintering and aggregation.

Recently, researchers have found that the use of porous metal–organic frameworks (MOFs) as supports to form monodispersed and isolated metal nanoparticles is an effective strategy. MOFs have been utilized as a new type of support for metal NPs as they have multiple outstanding properties such as controllable topologies, structures and geometries, porosities, and exceptionally high surface areas.[216,217] Such distinctive properties are deemed crucial to obtain well-dispersed nanoparticles hence decreasing the possibility of active phase sintering.

Aside from MOF implementation as catalytic supports and somehow stabilizing frameworks, recent studies validated MOFs as catalysts themselves, in which case, metallic centres or pseudo-organic linkers such as porphyrins are responsible for the catalytic activity.[218] Alternatively, MOFs have been successfully applied as precursor materials to design highly active RWGS catalysts *via* MOF decomposition.[219] Although significant achievements have been obtained in the field of catalysis by MOFs, the study on the CO_2 conversion *via* a

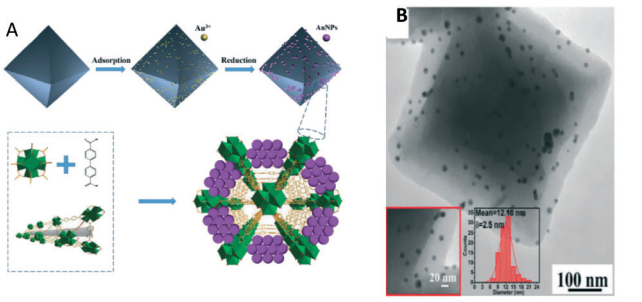

Fig. 17 A) Schematic of the catalyst synthesis strategy; B) transmission electron microscopy (TEM) images of Au@UIO-67 (reproduced from ref. 220 with permission from the Royal Society of Chemistry, copyright 2021).

RWGS reaction using these emerging materials is still in its early stages.

Xu *et al.* in 2017 reported the first example of a MOF-catalysed RWGS reaction, using Au@MOF composite catalysts.[220] Zr(IV)-based MOF UiO-67 was selected as a support owing to its porosity, high surface area and high thermal stability (≈500 °C). For the active phase, Au^{3+} was adsorbed into the surface cavities of UiO-67, and during the reduction process, AuNPs were controllably grown on the UiO-67 surface simultaneously accompanied by their self-immobilization in the cavities or the surface pores, resulting in highly isolated and well-dispersed AuNPs on MOF UiO-67 (Fig. 17A).

In this study, TEM images of the post-RWGS reaction sample were reported confirming the excellent dispersion of AuNPs within the engineered Au@UiO-67-catalysts (Fig. 17B). These cleverly designed catalysts serve as a reassuring example of sintering mitigation of AuNPs when framed within the MOF structure despite the high temperature needed for the RWGS.

Along with resistance to sintering, interesting catalytic results were obtained for the Au@UiO-67 composite, which merits further discussion. Outstanding CO selectivity was reached (96.5%), and only a trace of CH_4 was detected. Fig. 18 shows the influence of the main reaction parameter on the overall performance. The CO_2 conversion of Au@UiO-67 for the RWGS reaction gradually increased upon increasing the reaction temperature due to the endothermic nature of the reaction (black bars). Below 300 °C, the reaction showed almost no conversion because of the stable nature of the C–O bond in the CO_2 previously mentioned. Above 350 °C, the CO_2 conversion increased notably reaching 30% at 408 °C. Regarding pressure studies (red bars), the CO_2 conversion of the RWGS reaction gradually increased with pressure. Despite the RWGS being in principle unaffected by pressure if we stick to Le Chatelier's principle, the positive effect of pressure was ascribed to the greater reactant concentration being in contact with Au nanoparticles' active sites at high pressure, improving the overall conversion. The impact of the reactant feeding ratio (blue bars) was also studied and higher CO_2 conversion was obtained upon increasing the $H_2:CO_2$ volume ratio, in good agreement with studies conducted with the thermodynamic process.[221]

Finally, the authors studied the effect of Au loading (green bars). Interestingly a maximum CO_2 conversion was observed over the Au-promoted UiO-67 MOF when 2.4 wt% of Au was considered. Beyond this point, the conversion drops. Generally speaking, the main advantage of this kind of material is the porous nature of the MOFs, which promotes the formation of isolated and well-dispersed active phase nanoparticles. However, AuNPs deposited on UiO-67 slightly tend to migrate and agglomerate, reducing the number of active sites at high temperatures. Therefore, when the AuNP loading is high, the overcrowding presence of AuNPs increased the possible migration and sintering at the expense of CO_2 conversion. Additionally, a longevity test was carried out showing that the Au@UiO-67 catalyst exhibited relatively stable catalytic performance, indicating that AuNPs do not easily aggregate on the surface when the optimum gold loading is considered.

Hence it is clear that highly dispersed Au nanoparticles successfully loaded onto monodisperse octahedra of UiO-67 work very well for the RWGS. Herein MOF functionalities allow the incorporation of different nanoparticles in a non-agglomerated fashion and are capable of controlling the spatial distribution of nanoparticles in this material. Furthermore, engineered AuNP@UiO-67 composites encompass the benefits of the molecular sieving and porous behaviour characteristic of the UiO-67 matrix and the functional behaviour characteristic of dispersed and isolated gold particles resulting in a very promising system for CO_2 conversion *via* the RWGS.

Another interesting approach consists of the utilisation of MOFs for active material encapsulation. In this way, taking advantage of the confined pore space within the MOF structure, metal nanoparticle sintering and poisoning are prevented. Under these premises, Zheng and co-workers used MOF UiO-66 to encapsulate core–shell Au@Pd nanospheres controlling its morphology and gaining nanoparticle functionality (Fig. 19).[222] Furthermore, they benefit from the microporous nature of UiO-66 assisting in the adsorption of Pt nanoparticles over the MOF surface. Such improved adsorption enhances the interaction between Pt and UIO-66 and favours the formation of isolated and well-dispersed Pt active sites.

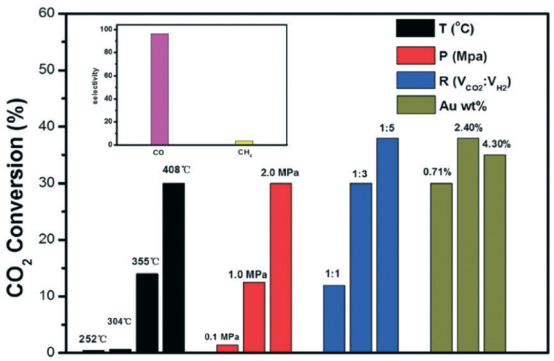

Fig. 18 CO_2 conversion at different temperatures (in black), pressures (in red), volume ratios (in blue) and Au contents (in green) for the RWGS reaction. Selectivities to CO and CH_4 (inset) (reproduced from ref. 220 with permission from the Royal Society of Chemistry, copyright 2021).

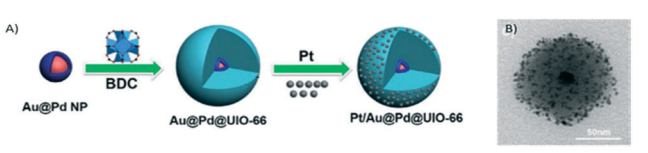

Fig. 19 A) Synthetic route to produce the Pt/Au@Pd@UiO-66 composite. B) TEM image (reproduced from ref. 222 with permission from John Wiley and Sons, copyright 2021).

The as-obtained Pt/Au@Pd@UiO-66 composites were tested in the RWGS reaction using a continuous flow fixed bed reactor. At 300 °C, 2 MPa, a $H_2:CO_2$ molar ratio of 4 : 1, and a gas hourly space velocity of 24 000 mL g^{-1} h^{-1}, the CO_2 conversion was 10% for this material. Elevated temperatures favoured the conversion of CO_2 reaching 35.3% at 400 °C, but the selectivity to CO decreased with the increase of the temperature, mainly due to the heat absorbed by the endothermic RGWS reaction and the increased amount of CH_4 derived from the unavoidable competitive methanation reaction. The stability performance of the Pt/Au@Pd@UiO-66 catalyst was excellent at 400 °C for over 30 h of continuous operation (Fig. 20). Pt nanoparticles still remained highly dispersed, and Au@Pd remained localized in the UIO-66 centres adopting a one-to-one fashion. Nevertheless, at 400 °C, the framework of UIO-66 collapsed. XRD analysis showed that UIO-66 had turned into ZrO_2, and the aggregation of Pt led to clusters of *ca.* 5.9 nm on the oxide surface. This particle size was still small, so the catalyst maintained an excellent catalytic performance. The bimetal core Au@Pd displayed a robust structure resulting in the observed outstanding stability for continuous RWGS runs.

The relatively low thermal stability of MOFs could in principle be a drawback for the RWGS given the exothermic nature of the reaction requiring high temperatures to achieve high CO_2 conversion levels. Nevertheless, the outstanding chemical and structural features of MOFs might outbalance this disadvantage since as demonstrated by Zheng and co-workers, a low-temperature RWGS catalyst can be designed based on a metal-doped MOF structure.[222] As mentioned above implementation of low-temperature RWGS catalysts represents a step ahead on this technology if a downstream process such as FTS is envisaged to close the CO_2 to fuel cycle. Herein MOFs present unique advantages, and their study deserves further attention.

Within the low-temperature RWGS contact, Gutterød *et al.* conducted CO_2 hydrogenation over Pt-containing UiO-67 Zr-MOFs at low-temperatures, 220–280 °C, and ambient pressure.[223] For this catalyst, Pt was introduced into the UiO-67 Zr-MOF framework by grafting it to a bipyridine-based linker, which constituted 5% of the framework linkers. Pt nanoparticles were obtained by pre-activation in a H_2/Ar flow

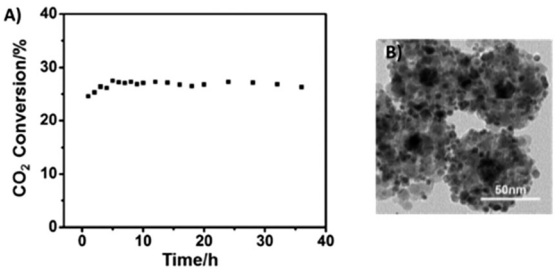

Fig. 20 A) RWGS reaction stability test at 400 °C and B) TEM image after catalysis at a temperature of 400 °C of the Pt/Au@Pd@UiO-66 catalyst (reproduced from ref. 222 with permission from John Wiley and Sons, copyright 2021).

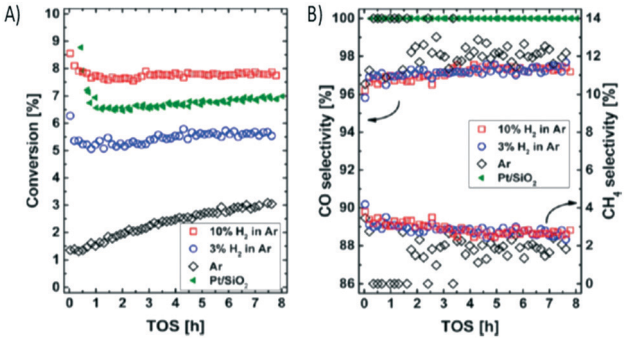

Fig. 21 A) Conversion (%) *versus* time on stream (hours) observed for UiO-67–Pt-PSF(M) under reference conditions after pre-activation at 350 °C (1 h) in a flow of Ar with 0, 3, and 10% H_2. B) CO and CH_4 selectivities. The conversion and CO selectivity observed for a reference material, Pt/SiO_2, is marked with green tilted triangles (reproduced from ref. 223 with permission from the American Chemical Society, copyright 2021).

at 350 °C. It was evidenced that the UiO-67 Zr-MOF framework was stable during all treatments.

Experimental results showed that the CO_2 conversion was positively correlated with the degree of Pt reduction over the MOF (Fig. 21). A CO selectivity above 90% was obtained under all tested conditions, a highly commendable achievement given that in the low temperature range CH_4 is the preferred product according purely to thermodynamics.[224] The authors observed a low reaction order in pH_2 and pCO_2, suggesting high coverage of the active site(s). Finally they compared the UiO-67–Pt catalysts with a conventional Pt/SiO_2 catalyst showing very similar activation energy, with E_{app} = 50 ± 3 kJ mol^{-1} suggesting that CO_2 hydrogenation follows the same mechanism over the two materials.

The use of MOFs as precursors of metal catalysts is another well-established field of research that is worth exploring for the preparation of highly dispersed supported active phases for the RWGS reaction. MOF derivatives, namely, metal oxide/carbon composites, tend to display enhanced catalytic activity and stability.[225,226] This customised transformation of MOFs into high performance catalysts combines crystal engineering techniques while meeting the requirements from a chemical engineering perspective.

In a nutshell, the process consists of carefully controlled MOF thermal decomposition. During the thermal treatment, the metal ions present in the MOFs are transformed into metallic or metal oxide nanoparticles, and the organic linkers form carbonaceous structures that can act as supports facilitating the active phase dispersion.

In a recent proof-of-concept example, Ronda-Lloret *et al.* used a copper-based MOF as a metallic precursor and CeO_2 as a final support/promoter to prepare a stable and active CuO_x/CeO_2 catalyst for the RWGS reaction (Fig. 22).[227] In this work, a Cu-MOF (Basolite® C300) was impregnated with a ceria precursor and then pyrolyzed using different conditions

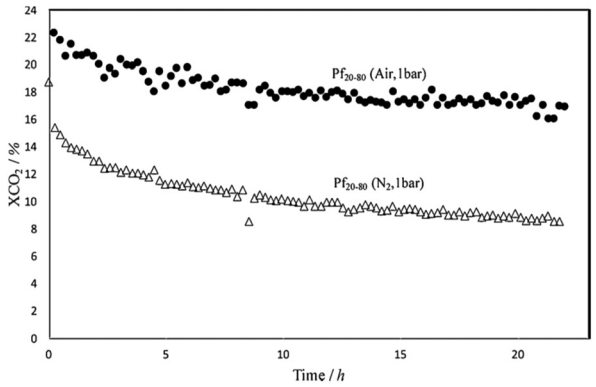

Fig. 22 Comparison of the catalytic performance of the samples Pf20–80 (air, 1 bar) and Pf20–80 (N_2, 1 bar) in RGWS (samples prepared by fast pyrolysis, Pf, with a molar ratio of 20Cu : 80Ce) (reproduced from ref. 227 with permission from Elsevier, copyright 2021).

and procedures. An oxidative atmosphere keeps copper oxidized during the decomposition and prevents active phase sintering. The presence of air in the decomposition induces the formation of copper oxide species, which have been demonstrated to be more resistant to sintering than metallic copper, thus favouring the interaction with the CeO_2 support. Herein the authors found that the pyrolysis method determined the dispersion of the oxidized copper species on the ceria surface, which, in turn, controls the catalytic activity and selectivity of these MOF-derived catalysts in the RWGS reaction.

Well-established industrial catalysts such as the Cu–Zn combination which is widely applied in methanol synthesis and industrial WGS reactions can also be re-engineered using MOFs as precursors. Zhang *et al.* and co-workers designed Cu/Zn nanoparticles in a carbon matrix material following this approach.[228] In this work, Zn-doped Cu–BTC was pyrolyzed at 500 °C under an argon atmosphere. The encapsulation of the obtained Cu/Zn NPs in the porous carbon matrix protected the NPs from aggregation and sintering, leading to superior stability of the catalysts in the RWGS reaction. Furthermore, enhanced synergistic effects between Cu and Zn were achieved increasing the catalytic activity due to the well mixed Cu and Zn from pyrolysis. Additionally, the authors carried out a study of the dependence of the catalytic activity on the pellet size, which revealed the importance of fine-tuning the crystal sizes of the pyrolysis precursors, which allows eliminating an additional step of catalyst forming. The highest CO_2 conversion (5%) and CO selectivity (100%) were exhibited by a Cu/Zn@C sample with a submillimeter-size at 500 °C and 1 bar (H_2 : CO_2 = 3 : 1). Additionally, the catalyst remained stable and active for over 20 hours.

4.3. Dry reforming of methane (DRM)

Research on catalytic carbon dioxide reforming of methane by MOF-based materials has only just begun, and hence the literature in this area is scarce. Compared with other reference catalytic materials, such as metal oxides, zeolites, metal alloys, *etc.*, there are still obvious gaps in stability and activity for MOF-based catalysts in this direct gas phase CO_2 conversion reaction. However, from the existing reports, the prospects are very promising.

Considering the thermal conditions of DRM (>600 °C), MOFs with low thermal stability (<400 °C) rapidly degrade, resulting in a structure collapse. Hence the way to use MOFs is as precursors of highly active catalysts in the DRM reaction.

This very strategy was successfully utilised by Karam *et al.* who utilised an Al-containing MIL-53 metal–organic framework with a very high surface area (S_{BET} = 1130 m^2 g^{-1}) as a sacrificial template to prepare a nickel-alumina-based catalyst (Ni^0Al_{MIL}).[229] After the calcination procedure, a porous uniform spinel phase with Ni nanoparticles embedded in the Al_2O_3-based matrix was obtained. This led after reduction to a porous lamellar γ-Al_2O_3 material with small Ni^0 nanoparticles homogeneously dispersed and stabilized within the support. This MOF as a sacrificial framework provided materials with a higher surface area than those generally encountered in the domain, and the interlamellar spaces provided additional stabilization to the confined nickel nanoparticles, which in turn inhibited carbon nanotube formation during the reaction.

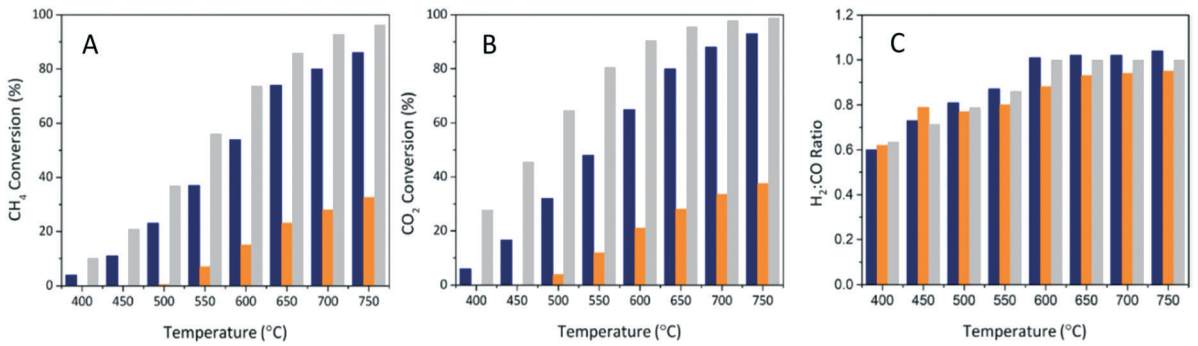

Fig. 23 (A) CH_4, (B) CO_2 conversions, and (C) H_2 : CO product ratio during DRM at 400 °C to 750 °C over *in situ* reduced (800 °C/2 h): (blue) Ni^0Al_{MIL} and (orange) Ni^0/Al (conventional γ-alumina). Grey columns are the calculated values at the thermodynamic equilibrium (reproduced from ref. 229 with permission from John Wiley and Sons, copyright 2021).

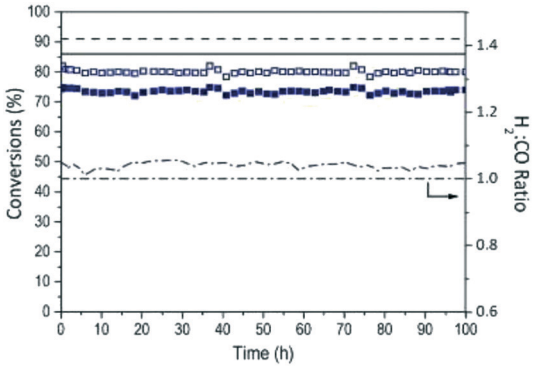

Fig. 24 CO_2 (filled squares) and CH_4 (empty squares) conversions as well as H_2 : CO ratios (dash-dotted line) measured during 100 h of reaction for Ni^0/Al_{MIL} (the black dash-dotted line represents H_2 : CO = 1). Black continuous and dashed lines are the calculated values at the thermodynamic equilibrium for CH_4 and CO_2 conversions, respectively (reproduced from ref. 229 with permission from John Wiley and Sons, copyright 2021).

The Ni/Al_{MIL} catalyst demonstrated a superior performance (CH_4 and CO_2 conversion) over a benchmark catalyst in the whole studied temperature range (Fig. 23). As for the H_2 : CO molar ratio, values for Ni^0/Al (conventional γ-alumina) are always lower than the thermodynamic threshold (which is 1.0 due to the nature of the reaction) primarily due to the competition with the RWGS reaction. Interestingly such a H_2/CO ratio becomes closer to 1 for Ni^0/Al_{MIL}, indicating a superior selectivity to the targeted reaction.

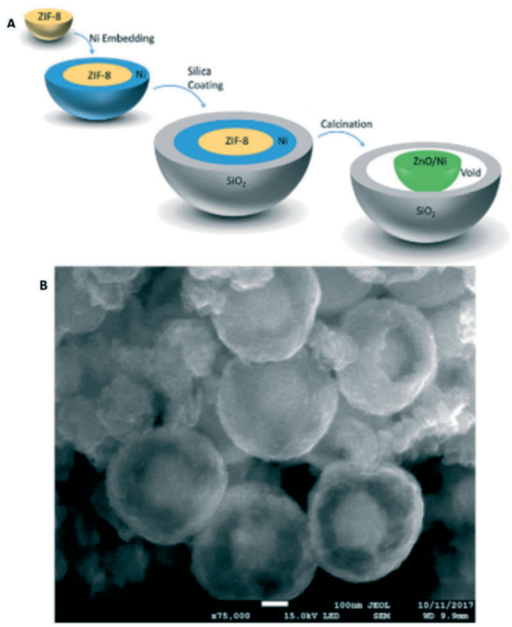

Fig. 25 A) Schematic illustration of the synthesis procedure of yolk–shell catalysts. B) SEM image of the resultant ZnO/Ni@*m*-SiO_2 yolk–shell particles, confirming successful encapsulation (reproduced from ref. 178 with permission from the Royal Society of Chemistry, copyright 2021).

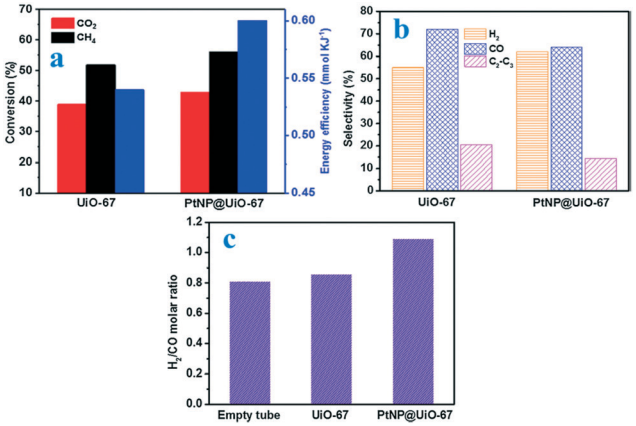

Fig. 26 Effect of different catalysts on (a) conversions and energy efficiency, (b) H_2/CO molar ratio and (c) selectivities to CO, H_2 and hydrocarbons during the plasma assisted catalytic DRM (at a power of 11 W, a feed flow rate of 100 ml min^{-1} and CH_4/CO_2 molar ratio) (reproduced from ref. 230 with permission from Elsevier, copyright 2021).

Furthermore, this material showed outstanding catalytic stability after 100 h of reaction with limited occurrence of side reactions (Fig. 24).

Following a similar MOF templating strategy, our team recently reported the synthesis of mesoporous ZnO/Ni@*m*-SiO_2 yolk–shell particles using a ZIF-8 MOF as a structural template.[178] Briefly ZIF-8 was impregnated with a Ni precursor to form the core of the yolk–shell particles (Fig. 25). In this novel system, Ni/ZnO was selected as active sites constituting the yolk structure while porous silica was selected as the shell material. The advantages of these configurations are two-fold: (i) the shell acts as a barrier to prevent the blocking of the active sites through coke formation and (ii) the confinement effect ascribed to the encapsulation of the active centres prevents Ni sintering. In this seminal work we demonstrated the superiority of Ni

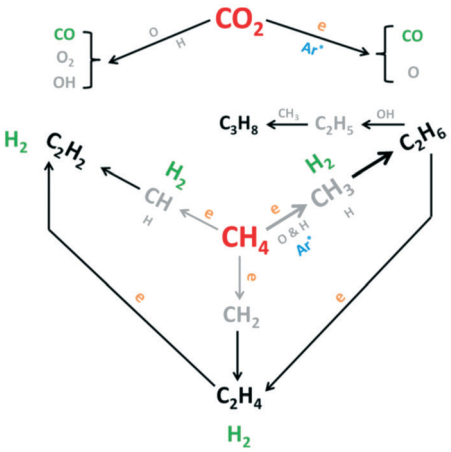

Fig. 27 Main reaction pathways in plasma-assisted catalytic DRM (reproduced from ref. 230 with permission from Elsevier, copyright 2021).

based yolk–shell catalysts over standard Ni catalysts which are traditionally used in reforming units.

Perhaps more interestingly, a recent study reports a MOF material that directly serves as a chemically and thermally stable support in a particular case. R. Vakili *et al.* accomplished plasma-assisted dry reforming over a PtNP@UiO-67 catalyst (Fig. 26).[230] The authors were able to break through the thermodynamic limit of the DRM by the energetic electron activation of reactant molecules rather than the traditional thermal activation. The highly porous UiO-67 (>2000 m^2 g^{-1}) was stable under plasma conditions showing no significant changes in its properties under conditions of different treatment times, discharge powers and gases. Furthermore, this MOF favored the dispersion of fine Pt particles. It has to be highlighted that the UiO-67 MOF facilitated the plasma formation and surface discharges in the discharge zone, coupling with the Pt particles to enhance the CH_4 and CO_2 conversion and syngas production due to the presence of surface reactions (Fig. 27).

5. Concluding remarks and future perspectives

CO_2 capture and conversion technologies rely on highly effective materials whose chemistry and engineering aspects must be finely customized to maximise the overall process performance. In this scenario, MOF materials emerge as revolutionary systems with unique features opening new research avenues for both CO_2 capture and catalytic CO_2 conversion. A great deal of work has been done so far by the chemistry and engineering communities resulting in promising breakthroughs in terms of CO_2 capture capacity of custom-made MOFs when compared to the state-of-the-art materials. Herein aspects such as the synthesis method choice, the addition of promoters and careful control of the acid-based properties of the MOFs are crucial. Also, engineering aspects such as cyclability, regeneration and isosteric heat must be considered to fully describe the behaviour of a MOF for CO_2 capture applications. Support from *operando* studies is deemed fundamental to discern the system dynamics during CO_2 capture and hence to evaluate a rational design of high performance MOFs.

As for the gas phase catalytic CO_2 conversion, the results reported so far are certainly encouraging pointing a bright future for MOFs in core processes such as CO_2 methanation, RWGS and DRM reactions. MOFs benefit from the confinement effect preventing the occurrence of frequent problems in heterogeneous catalysis such as carbon poisoning and metallic particle sintering. In addition, their framework allows outstanding active phase dispersion favoring high CO_2 conversion levels outperforming standard catalysts for these reactions.

Besides the successful results, we have identified some gaps and challenges that require further attention if real application is envisaged. The utilization of realistic or surrogate flue gas streams for both CO_2 capture and conversion is greatly lacking in the open literature. The presence of water, nitrogen, and sulphur oxides among other impurities may jeopardize the adsorption and catalytic features, and they must be studied to seriously consider MOFs for commercial applications in CO_2 capture/upgrading processes. When it comes to catalysis and endothermic processes such as DRM, the thermal stability of MOFs imposes a challenge which should be overcome. Despite these difficulties, MOFs and CO_2 conversion/scrubbing processes seem to share a common destiny, and there is no doubt that this family of unique materials is meant to play a crucial role in the implementation of disruptive low-carbon technologies to combat global warming.

List of acronyms and abbreviations

aTZ	(1*H*-1,2,4-Triazol-3-yl)amide
bbIm	5(6)-Bromobenzimidazole
BDC	1,4-Benzenedicarboxylate
bIM	Benzimidazole
BPDC	Biphenyl-1,4-dicarboxylate
BPEB	1,4-Bis(1*H*-pyrazol-4-ylethynyl)benzene
BPTC	3,3′,5,5′-Biphenyltetracarboxylate
bpy	2,2′-Bipyridine
brbIm	6-Bromobenzylimidazole
BTB	1,3,5-Tris(4-carboxyphenyl)benzene
BTC	Benzene-1,3,5-tricarboxylate
CALF-33	$[Cu_3(L1\text{-}Et_2H)_2]_n$ L1 = 1,3,5-tris(4-bromophenyl) benzene
cbIm	5(6)-Chlorobenzimidazole
CCS	CO_2 capture and storage
CCU	Carbon dioxide capture and utilisation
cnIm	4-Cyanoimidazole
CPO	Coordination polymer of Oslo
DMF	*N*,*N*-Dimethyl formamide
DOBCO	2,5-Dihydroxyterephthalic acid
EDS	1,2-Ethanedisulfonate
HKUST	Hong Kong University of Science and Tech.
HKUST-1	$[Cu_3(btc)_2(H_2O)_3]$
HPDC	4,5,9,10-Tetrahydropyrene-2,7-dicarboxylate
HT	High-throughput
IRMOF	Isoreticular MOF
IRMOF-1	$Zn_4O(BDC)_3$
IRMOF-11	$Zn_4O(HPDC)_3$
IRMOF-3	$[Zn_4O(NH_2\text{-}BDC)_3]$
IRMOF-6	$Zn_4O(cyclobutyl\text{-}BDC)_3$
IRMOF-74-III	$[Mg_2(DH_3PhDC)]$
JUC	Jilin University China
JUC-150	$[Ni_2(L\text{-}asp)_2(pz)]$
L-asp	L-aspartic acid
LIMF-26	$Fe_3(TCDC)_3(H_2O)_3$
mbIm	5(6)-Methylbenzimidazole
M-CPO-27	$[M_2(dobdc)(H_2O)_2]$ (M = Mg^{2+}, Ni^{2+}, Co^{2+}, Zn^{2+})
MEA	Monoethanolamide
MeIM	Methyl-imidazole
MIL	Matériaux de l'Institut Lavoisier

MIL-100	$Fe_3O(H_2O)2F\{C_6H_3(CO_2)_3\}_2{\cdot}nH_2O$ ($n \approx 14.5$)
MIL-101	$Cr_3F(H_2O)_2O(BDC)_3{\cdot}nH_2O$ ($n \approx 25$)
MIL-96	$Al_{12}O(OH)_{18}(H_2O)_3(Al_2(OH)_4)[btc]_6{\cdot}24H_2O$
MOF	Metal–organic framework
MOF-177	$[Zn_4O(BTB)_2]$
MOF-2	$Zn(BDC)(DMF)(H_2O)$
MOF-5	$[Zn_4O(BDC)_3]$
MOF-505	$[Cu_2(bptc)(H_2O)_2(DMF)_3(H_2O)]$
MUF	Massey University Framework
MUF-15	$[Fe_2(O_2)(dobdc)]$
nbIm	5-Nitrobenzimidazole
nbIM	Nitro-benzene imidazole
NH_2-MIL-125	$[Ti_8O_8(OH)_4(NH_2\text{-}BDC)_6]$
NH_2-MIL-53	$[Al(OH)(NH_2\text{-}BDC)]_n$
NH_2–UiO-66	$[Zr_6O_4(OH)_4(NH_2\text{-}BDC)_6]$
nIm	2-Nitroimidazole
nIM	5-Nitroimidazole
NOTT-202a	$(Me_2NH_2)_{1.75}[In(L)]_{1.75}(DMF)_{12}(H_2O)_{10}$ (H_4L = biphenyl-3,30,5,50-tetra-(phenyl-4-carboxylic acid))
NU-100	$Cu_3(TTEI)$
PCN	Porous coordination network
PCN-61	$Cu_3(H_2O)_3(btei)$
PCN-66	$Cu_3(H_2O)_3(ntei)$
PCN-68	$Cu_3(H_2O)_3(ptei)$
PSF	Poly(bisphenol-A sulfone)
PVDF	Polyvinylidene fluoride
pz	Pyrazine
SBU	Secondary building unit
SNU	Seoul National University
SNU-100	$[Zn_3(TCPT)_2(HCOO)][NH_2(CH_3)_2]$
TCDC	2,3,5,6-Tetrachloride terephthalate
TCPT	2,4,6-Tris-(4-carboxy-phenoxy)-1,3,5-triazine
TMOF-1	$[Cu(4,40\text{-}bpy)_2(EDS)]_n$
TZ	3,5-Bis(trifluoromethyl)-1,2,4-triazolate
UiO	Universitetet i Oslo
UiO-66	$[Zr_6O_4(OH)_4(BDC)_6]$
UiO-67	$[Zr_6O_4(OH)_4(BPDC)_6]$
ZIF	Zeolitic imidazolate framework
ZIF-300	$Zn(2\text{-}mIm)_{0.86}(bbIm)_{1.14}$
ZIF-301	$Zn(2\text{-}mIm)_{0.94}(cbIm)_{1.06}$
ZIF-302	$Zn(2\text{-}mIm)_{0.67}(mbIm)_{1.33}$
ZIF-68	Zn(bIm)(nIm)
ZIF-69	Zn(cbIm)(nIm)
ZIF-7	$Zn(bIM)_2$
ZIF-70	$Zn(Im)_{1.13}(nIm)_{0.87}$
ZIF-78	Zn(nbIm)(nIm)
ZIF-79	Zn(mbIm)(nIm)
ZIF-8	$Zn(MeIM)_2$
ZIF-81	Zn(brbIm)(nIm)
ZIF-82	Zn(cnIm)(nIm)

Author contributions

The authors equally contributed to this work.

Conflicts of interest

There are no conflicts to declare.

Acknowledgements

Financial support for this work was provided by the Spanish Ministry of Science and Spanish Ministry of Science and Innovation through the project RYC2018-024387-I as well as the project PID2019-108502RJ-I00. This work was also partially funded by the University of Seville *via* the VI PPIT grant scheme for talented researchers.

References

1 J. C. M. Farla, C. A. Hendriks and K. Blok, *Clim. Change*, 1995, **29**, 439–461.
2 G. Cui, J. Wang and S. Zhang, *Chem. Soc. Rev.*, 2016, **45**, 4307–4339.
3 S. Wang, S. Yan, X. Ma and J. Gong, *Energy Environ. Sci.*, 2011, **4**, 3805.
4 M. K. Mondal, H. K. Balsora and P. Varshney, *Energy*, 2012, **46**, 431–441.
5 A. Corma, H. García and F. X. Llabrés i Xamena, *Chem. Rev.*, 2010, **110**, 4606–4655.
6 J. L. C. Rowsell and O. M. Yaghi, *Microporous Mesoporous Mater.*, 2004, **73**, 3–14.
7 S. S. Kaye, A. Dailly, O. M. Yaghi and J. R. Long, *J. Am. Chem. Soc.*, 2007, **129**, 14176–14177.
8 F. X. Llabrés i Xamena and J. Gascon, in *Metal Organic Frameworks as Heterogeneous Catalysts*, 2001, pp. 1–5.
9 H.-C. Zhou, J. R. Long and O. M. Yaghi, *Chem. Rev.*, 2012, **112**, 673–674.
10 Q. Wang, J. Bai, Z. Lu, Y. Pan and X. You, *Chem. Commun.*, 2016, **52**, 443–452.
11 K. Eum, K. C. Jayachandrababu, F. Rashidi, K. Zhang, J. Leisen, S. Graham, R. P. Lively, R. R. Chance, D. S. Sholl, C. W. Jones and S. Nair, *J. Am. Chem. Soc.*, 2015, **137**, 4191–4197.
12 W.-Y. Gao, Y. Chen, Y. Niu, K. Williams, L. Cash, P. J. Perez, L. Wojtas, J. Cai, Y.-S. Chen and S. Ma, *Angew. Chem., Int. Ed.*, 2014, **53**, 2615–2619.
13 J. Yu, L.-H. Xie, J.-R. Li, Y. Ma, J. M. Seminario and P. B. Balbuena, *Chem. Rev.*, 2017, **117**, 9674–9754.
14 A. A. Olajire, *Energy*, 2010, **35**, 2610–2628.
15 A. Rabenau, *Angew. Chem., Int. Ed. Engl.*, 1985, **24**, 1026–1040.
16 N. Stock and S. Biswas, *Chem. Rev.*, 2012, **112**, 933–969.
17 R. Banerjee, A. Phan, B. Wang, C. Knobler, H. Furukawa, M. O'Keeffe and O. M. Yaghi, *Science*, 2008, **319**, 939–943.
18 P. Küsgens, M. Rose, I. Senkovska, H. Fröde, A. Henschel, S. Siegle and S. Kaskel, *Microporous Mesoporous Mater.*, 2009, **120**, 325–330.
19 S. J. Garibay and S. M. Cohen, *Chem. Commun.*, 2010, **46**, 7700.
20 X. Zhu, B. Li, J. Yang, Y. Li, W. Zhao, J. Shi and J. Gu, *ACS Appl. Mater. Interfaces*, 2015, **7**, 223–231.

21 S. H. Jhung, J. H. Lee and J. S. Chang, *Bull. Korean Chem. Soc.*, 2005, **26**, 880–881.
22 R. Ameloot, L. Stappers, J. Fransaer, L. Alaerts, B. F. Sels and D. E. De Vos, *Chem. Mater.*, 2009, **21**, 2580–2582.
23 T. Friščić, *J. Mater. Chem.*, 2010, **20**, 7599.
24 S. L. James, C. J. Adams, C. Bolm, D. Braga, P. Collier, T. Friščić, F. Grepioni, K. D. M. Harris, G. Hyett, W. Jones, A. Krebs, J. Mack, L. Maini, A. G. Orpen, I. P. Parkin, W. C. Shearouse, J. W. Steed and D. C. Waddell, *Chem. Soc. Rev.*, 2012, **41**, 413–447.
25 D. Braga and F. Grepioni, *Chem. Commun.*, 2005, 3635.
26 L.-G. Qiu, Z.-Q. Li, Y. Wu, W. Wang, T. Xu and X. Jiang, *Chem. Commun.*, 2008, 3642.
27 B. Rungtaweevoranit, C. S. Diercks, M. J. Kalmutzki and O. M. Yaghi, *Faraday Discuss.*, 2017, **201**, 9–45.
28 M. Ding, R. W. Flaig, H.-L. Jiang and O. M. Yaghi, *Chem. Soc. Rev.*, 2019, **48**, 2783–2828.
29 G. T. Rochelle, *Science*, 2009, **325**, 1652–1654.
30 L.-M. Dion, M. Lefsrud and V. Orsat, *Biomass Bioenergy*, 2011, **35**, 3422–3432.
31 V. Bon, I. Senkovska, M. S. Weiss and S. Kaskel, *CrystEngComm*, 2013, **15**, 9572.
32 F. Drache, V. Bon, I. Senkovska, C. Marschelke, A. Synytska and S. Kaskel, *Inorg. Chem.*, 2016, **55**, 7206–7213.
33 Z. Kang, M. Xue, L. Fan, L. Huang, L. Guo, G. Wei, B. Chen and S. Qiu, *Energy Environ. Sci.*, 2014, **7**, 4053–4060.
34 Y.-Q. Lan, S.-L. Li, H.-L. Jiang and Q. Xu, *Chem. – Eur. J.*, 2012, **18**, 8076–8083.
35 C. A. Trickett, A. Helal, B. A. Al-Maythalony, Z. H. Yamani, K. E. Cordova and O. M. Yaghi, *Nat. Rev. Mater.*, 2017, **2**, 17045.
36 Y. Lin, C. Kong, Q. Zhang and L. Chen, *Adv. Energy Mater.*, 2017, **7**, 1601296.
37 K. C. Stylianou and W. L. Queen, *CHIMIA International Journal for Chemistry*, 2015, **69**, 274–283.
38 D. Andirova, C. F. Cogswell, Y. Lei and S. Choi, *Microporous Mesoporous Mater.*, 2016, **219**, 276–305.
39 A. R. Millward and O. M. Yaghi, *J. Am. Chem. Soc.*, 2005, **127**, 17998–17999.
40 H. W. B. Teo, A. Chakraborty and S. Kayal, *Appl. Therm. Eng.*, 2017, **110**, 891–900.
41 J. Li, C. Zhu, Z. Qiao, X. Chen, W. Wei, H. Ji and K. Sohlberg, *Appl. Surf. Sci.*, 2016, **385**, 578–586.
42 W. L. Queen, M. R. Hudson, E. D. Bloch, J. A. Mason, M. I. Gonzalez, J. S. Lee, D. Gygi, J. D. Howe, K. Lee, T. A. Darwish, M. James, V. K. Peterson, S. J. Teat, B. Smit, J. B. Neaton, J. R. Long and C. M. Brown, *Chem. Sci.*, 2014, **5**, 4569–4581.
43 X. Kong, E. Scott, W. Ding, J. A. Mason, J. R. Long and J. A. Reimer, *J. Am. Chem. Soc.*, 2012, **134**, 14341–14344.
44 C.-X. Chen, S.-P. Zheng, Z.-W. Wei, C.-C. Cao, H.-P. Wang, D. Wang, J.-J. Jiang, D. Fenske and C.-Y. Su, *Chem. – Eur. J.*, 2017, **23**, 4060–4064.
45 J. A. Mason, T. M. McDonald, T.-H. Bae, J. E. Bachman, K. Sumida, J. J. Dutton, S. S. Kaye and J. R. Long, *J. Am. Chem. Soc.*, 2015, **137**, 4787–4803.
46 O. K. Farha, A. Özgür Yazaydın, I. Eryazici, C. D. Malliakas, B. G. Hauser, M. G. Kanatzidis, S. T. Nguyen, R. Q. Snurr and J. T. Hupp, *Nat. Chem.*, 2010, **2**, 944–948.
47 D. Yuan, D. Zhao, D. Sun and H.-C. Zhou, *Angew. Chem., Int. Ed.*, 2010, **49**, 5357–5361.
48 T. Loiseau, L. Lecroq, C. Volkringer, J. Marrot, G. Férey, M. Haouas, F. Taulelle, S. Bourrelly, P. L. Llewellyn and M. Latroche, *J. Am. Chem. Soc.*, 2006, **128**, 10223–10230.
49 Z. Guo, H. Wu, G. Srinivas, Y. Zhou, S. Xiang, Z. Chen, Y. Yang, W. Zhou, M. O'Keeffe and B. Chen, *Angew. Chem., Int. Ed.*, 2011, **50**, 3178–3181.
50 S. Surblé, F. Millange, C. Serre, T. Düren, M. Latroche, S. Bourrelly, P. L. L. Llewellyn and G. Férey, *J. Am. Chem. Soc.*, 2006, **128**, 14889–14896.
51 N. MacDowell, N. Florin, A. Buchard, J. Hallett, A. Galindo, G. Jackson, C. S. Adjiman, C. K. Williams, N. Shah and P. Fennell, *Energy Environ. Sci.*, 2010, **3**, 1645.
52 H. R. Abid, J. Shang, H.-M. Ang and S. Wang, *Int. J. Smart Nano Mater.*, 2013, **4**, 72–82.
53 Q. Yang, A. D. Wiersum, P. L. Llewellyn, V. Guillerm, C. Serre and G. Maurin, *Chem. Commun.*, 2011, **47**, 9603.
54 P.-Q. Liao, X.-W. Chen, S.-Y. Liu, X.-Y. Li, Y.-T. Xu, M. Tang, Z. Rui, H. Ji, J.-P. Zhang and X.-M. Chen, *Chem. Sci.*, 2016, **7**, 6528–6533.
55 S. Couck, J. F. M. Denayer, G. V. Baron, T. Rémy, J. Gascon and F. Kapteijn, *J. Am. Chem. Soc.*, 2009, **131**, 6326–6327.
56 Y.-S. Bae, O. K. Farha, A. M. Spokoyny, C. A. Mirkin, J. T. Hupp and R. Q. Snurr, *Chem. Commun.*, 2008, 4135.
57 S.-N. Kim, J. Kim, H.-Y. Kim, H.-Y. Cho and W.-S. Ahn, *Catal. Today*, 2013, **204**, 85–93.
58 X. Si, C. Jiao, F. Li, J. Zhang, S. Wang, S. Liu, Z. Li, L. Sun, F. Xu, Z. Gabelica and C. Schick, *Energy Environ. Sci.*, 2011, **4**, 4522.
59 J. An, S. J. Geib and N. L. Rosi, *J. Am. Chem. Soc.*, 2010, **132**, 38–39.
60 B. Li, Z. Zhang, Y. Li, K. Yao, Y. Zhu, Z. Deng, F. Yang, X. Zhou, G. Li, H. Wu, N. Nijem, Y. J. Chabal, Z. Lai, Y. Han, Z. Shi, S. Feng and J. Li, *Angew. Chem., Int. Ed.*, 2012, **51**, 1412–1415.
61 T. M. McDonald, D. M. D'Alessandro, R. Krishna and J. R. Long, *Chem. Sci.*, 2011, **2**, 2022.
62 P.-Q. Liao, D.-D. Zhou, A.-X. Zhu, L. Jiang, R.-B. Lin, J.-P. Zhang and X.-M. Chen, *J. Am. Chem. Soc.*, 2012, **134**, 17380–17383.
63 R. W. Flaig, T. M. Osborn Popp, A. M. Fracaroli, E. A. Kapustin, M. J. Kalmutzki, R. M. Altamimi, F. Fathieh, J. A. Reimer and O. M. Yaghi, *J. Am. Chem. Soc.*, 2017, **139**, 12125–12128.
64 Z. Shi, Y. Tao, J. Wu, C. Zhang, H. He, L. Long, Y. Lee, T. Li and Y.-B. Zhang, *J. Am. Chem. Soc.*, 2020, **142**, 2750–2754.
65 R. Banerjee, H. Furukawa, D. Britt, C. Knobler, M. O. Keeffe and O. M. Yaghi, *J. Am. Chem. Soc.*, 2009, **131**, 3875–3877.
66 G. Zhang, G. Wei, Z. Liu, S. R. J. Oliver and H. Fei, *Chem. Mater.*, 2016, **28**, 6276–6281.
67 O. T. Qazvini, L. K. Macreadie and S. G. Telfer, *Chem. Mater.*, 2020, **32**, 6744–6752.

68 G. Chakraborty, P. Das and S. K. Mandal, *ACS Appl. Mater. Interfaces*, 2020, **12**, 11724–11736.
69 Q. Yang, S. Vaesen, F. Ragon, A. D. Wiersum, D. Wu, A. Lago, T. Devic, C. Martineau, F. Taulelle, P. L. Llewellyn, H. Jobic, C. Zhong, C. Serre, G. De Weireld and G. Maurin, *Angew. Chem., Int. Ed.*, 2013, **52**, 10316–10320.
70 K. Uemura, R. Matsuda and S. Kitagawa, *J. Solid State Chem.*, 2005, **178**, 2420–2429.
71 S. Bureekaew, S. Shimomura and S. Kitagawa, *Sci. Technol. Adv. Mater.*, 2008, **9**, 14108.
72 S. Horike, S. Shimomura and S. Kitagawa, *Nat. Chem.*, 2009, **1**, 695–704.
73 A. Schneemann, V. Bon, I. Schwedler, I. Senkovska, S. Kaskel and R. A. Fischer, *Chem. Soc. Rev.*, 2014, **43**, 6062–6096.
74 S. Ehrling, M. Mendt, I. Senkovska, J. D. Evans, V. Bon, P. Petkov, C. Ehrling, F. Walenszus, A. Pöppl and S. Kaskel, *Chem. Mater.*, 2020, **32**, 5670–5681.
75 Q. Dong, X. Zhang, S. Liu, R. Lin, Y. Guo, Y. Ma, A. Yonezu, R. Krishna, G. Liu, J. Duan, R. Matsuda, W. Jin and B. Chen, *Angew. Chem., Int. Ed.*, 2020, **59**, 22756–22762.
76 S. Aguado, G. Bergeret, M. P. Titus, V. Moizan, C. Nieto-Draghi, N. Bats and D. Farrusseng, *New J. Chem.*, 2011, **35**, 546–550.
77 C. Cuadrado-Collados, J. Fernández-Català, F. Fauth, Y. Q. Cheng, L. L. Daemen, A. J. Ramirez-Cuesta and J. Silvestre-Albero, *J. Mater. Chem. A*, 2017, **5**, 20938–20946.
78 J. van den Bergh, C. Gücüyener, E. A. Pidko, E. J. M. Hensen, J. Gascon and F. Kapteijn, *Chem. – Eur. J.*, 2011, **17**, 8832–8840.
79 P. K. Thallapally, J. Tian, M. Radha Kishan, C. A. Fernandez, S. J. Dalgarno, P. B. McGrail, J. E. Warren and J. L. Atwood, *J. Am. Chem. Soc.*, 2008, **130**, 16842–16843.
80 S. Yang, X. Lin, W. Lewis, M. Suyetin, E. Bichoutskaia, J. E. Parker, C. C. Tang, D. R. Allan, P. J. Rizkallah, P. Hubberstey, N. R. Champness, K. Mark Thomas, A. J. Blake and M. Schröder, *Nat. Mater.*, 2012, **11**, 710–716.
81 B. Li and B. Chen, *Sci. China: Chem.*, 2016, **59**, 965–969.
82 C. Wang, L. Li, J. G. Bell, X. Lv, S. Tang, X. Zhao and K. M. Thomas, *Chem. Mater.*, 2015, **27**, 1502–1516.
83 A. C. Forse, K. A. Colwell, M. I. Gonzalez, S. Benders, R. M. Torres-Gavosto, B. Blümich, J. A. Reimer and J. R. Long, *Chem. Mater.*, 2020, **32**, 3570–3576.
84 R. Zhang, J.-H. Huang, D.-X. Meng, F.-Y. Ge, L.-F. Wang, Y.-K. Xu, X.-G. Liu, M.-M. Meng, Z.-Z. Lu, H.-G. Zheng and W. Huang, *Dalton Trans.*, 2020, **49**, 5618–5624.
85 M. Eddaoudi, *Science*, 2002, **295**, 469–472.
86 H. Deng, S. Grunder, K. E. Cordova, C. Valente, H. Furukawa, M. Hmadeh, F. Gandara, A. C. Whalley, Z. Liu, S. Asahina, H. Kazumori, M. O'Keeffe, O. Terasaki, J. F. Stoddart and O. M. Yaghi, *Science*, 2012, **336**, 1018–1023.
87 L. Xie, M. Xu, X. Liu, M. Zhao and J. Li, *Adv. Sci.*, 2020, **7**, 1901758.
88 C. Mottillo and T. Friščić, *Angew. Chem., Int. Ed.*, 2014, **53**, 7471–7474.
89 A. C. Kizzie, A. G. Wong-Foy and A. J. Matzger, *Langmuir*, 2011, **27**, 6368–6373.
90 B. S. Gelfand, R. P. S. Huynh, R. K. Mah and G. K. H. Shimizu, *Angew. Chem., Int. Ed.*, 2016, **55**, 14614–14617.
91 Y.-S. Bae, J. Liu, C. E. Wilmer, H. Sun, A. N. Dickey, M. B. Kim, A. I. Benin, R. R. Willis, D. Barpaga, M. D. LeVan and R. Q. Snurr, *Chem. Commun.*, 2014, **50**, 3296–3298.
92 N. Ding, H. Li, X. Feng, Q. Wang, S. Wang, L. Ma, J. Zhou and B. Wang, *J. Am. Chem. Soc.*, 2016, **138**, 10100–10103.
93 W. Zhang, Y. Hu, J. Ge, H.-L. Jiang and S.-H. Yu, *J. Am. Chem. Soc.*, 2014, **136**, 16978–16981.
94 M. Ding, X. Cai and H.-L. Jiang, *Chem. Sci.*, 2019, **10**, 10209–10230.
95 N. T. T. Nguyen, H. Furukawa, F. Gándara, H. T. Nguyen, K. E. Cordova and O. M. Yaghi, *Angew. Chem., Int. Ed.*, 2014, **53**, 10645–10648.
96 M. Kalaj and S. M. Cohen, *ACS Cent. Sci.*, 2020, **6**, 1046–1057.
97 Y.-S. Bae, O. K. Farha, J. T. Hupp and R. Q. Snurr, *J. Mater. Chem.*, 2009, **19**, 2131.
98 C. H. Lau, R. Babarao and M. R. Hill, *Chem. Commun.*, 2013, **49**, 3634.
99 A. Kronast, S. Eckstein, P. T. Altenbuchner, K. Hindelang, S. I. Vagin and B. Rieger, *Chem. – Eur. J.*, 2016, **22**, 12800–12807.
100 C. Le Calvez, M. Zouboulaki, C. Petit, L. Peeva and N. Shirshova, *RSC Adv.*, 2016, **6**, 17314–17317.
101 M. Kalaj, K. C. Bentz, S. Ayala, J. M. Palomba, K. S. Barcus, Y. Katayama and S. M. Cohen, *Chem. Rev.*, 2020, **120**, 8267–8302.
102 Y. Zhang, X. Feng, S. Yuan, J. Zhou and B. Wang, *Inorg. Chem. Front.*, 2016, **3**, 896–909.
103 J. C. Moreton, M. S. Denny and S. M. Cohen, *Chem. Commun.*, 2016, **52**, 14376–14379.
104 M. S. Denny and S. M. Cohen, *Angew. Chem., Int. Ed.*, 2015, **54**, 9029–9032.
105 N. C. Su, D. T. Sun, C. M. Beavers, D. K. Britt, W. L. Queen and J. J. Urban, *Energy Environ. Sci.*, 2016, **9**, 922–931.
106 E. A. Feijani, H. Mahdavi and A. Tavasoli, *Chem. Eng. Res. Des.*, 2015, **96**, 87–102.
107 S. Sircar, R. Mohr, C. Ristic and M. B. Rao, *J. Phys. Chem. B*, 1999, **103**, 6539–6546.
108 H. Pan, J. A. Ritter and P. B. Balbuena, *Ind. Eng. Chem. Res.*, 1998, **37**, 1159–1166.
109 M. Dincă, A. Dailly, Y. Liu, C. M. Brown, D. A. Neumann and J. R. Long, *J. Am. Chem. Soc.*, 2006, **128**, 16876–16883.
110 J. An and N. L. Rosi, *J. Am. Chem. Soc.*, 2010, **132**, 5578–5579.
111 T. Li and N. L. Rosi, *Chem. Commun.*, 2013, **49**, 11385.
112 H. J. Park and M. P. Suh, *Chem. Sci.*, 2013, **4**, 685–690.
113 A. Raksajati, M. T. Ho and D. E. Wiley, *Ind. Eng. Chem. Res.*, 2013, **52**, 16887–16901.
114 P. Billemont, N. Heymans, P. Normand and G. De Weireld, *Adsorption*, 2017, **23**, 225–237.
115 A. L. Myers and J. M. Prausnitz, *AIChE J.*, 1965, **11**, 121–127.
116 K. S. Walton and D. S. Sholl, *AIChE J.*, 2015, **61**, 2757–2762.

117 Y.-S. Bae, K. L. Mulfort, H. Frost, P. Ryan, S. Punnathanam, L. J. Broadbelt, J. T. Hupp and R. Q. Snurr, *Langmuir*, 2008, **24**, 8592–8598.
118 F.-X. Coudert, C. Mellot-Draznieks, A. H. Fuchs and A. Boutin, *J. Am. Chem. Soc.*, 2009, **131**, 11329–11331.
119 B. Liu and B. Smit, *Langmuir*, 2009, **25**, 5918–5926.
120 J. E. Bara, C. J. Gabriel, S. Lessmann, T. K. Carlisle, A. Finotello, D. L. Gin and R. D. Noble, *Ind. Eng. Chem. Res.*, 2007, **46**, 5380–5386.
121 S. Farooq and D. M. Ruthven, *AIChE J.*, 1991, **37**, 299–301.
122 S. Farooq, H. Qinglin and I. A. Karimi, *Ind. Eng. Chem. Res.*, 2002, **41**, 1098–1106.
123 M. Khalighi, S. Farooq and I. A. Karimi, *Ind. Eng. Chem. Res.*, 2012, **51**, 10659–10670.
124 Z. Hu, M. Khurana, Y. H. Seah, M. Zhang, Z. Guo and D. Zhao, *Chem. Eng. Sci.*, 2015, **124**, 61–69.
125 L. Hamon, P. L. Llewellyn, T. Devic, A. Ghoufi, G. Clet, V. Guillerm, G. D. Pirngruber, G. Maurin, C. Serre, G. Driver, W. van Beek, E. Jolimaître, A. Vimont, M. Daturi and G. Férey, *J. Am. Chem. Soc.*, 2009, **131**, 17490–17499.
126 D. M. Ruthven, S. Farooq and K. S. Knaebel, *Pressure Swing Adsorption*, VCH Publishers, 1994.
127 S. Xiang, Y. He, Z. Zhang, H. Wu, W. Zhou, R. Krishna and B. Chen, *Nat. Commun.*, 2012, **3**(1), 954.
128 N. Al-Janabi, P. Hill, L. Torrente-Murciano, A. Garforth, P. Gorgojo, F. Siperstein and X. Fan, *Chem. Eng. J.*, 2015, **281**, 669–677.
129 Z. Hu, Y. Wang, S. Farooq and D. Zhao, *AIChE J.*, 2017, **63**, 4103–4114.
130 K. Sumida, D. L. Rogow, J. A. Mason, T. M. McDonald, E. D. Bloch, Z. R. Herm, T.-H. Bae and J. R. Long, *Chem. Rev.*, 2012, **112**, 724–781.
131 J. Canivet, A. Fateeva, Y. Guo, B. Coasne and D. Farrusseng, *Chem. Soc. Rev.*, 2014, **43**, 5594–5617.
132 H. Furukawa, F. Gándara, Y.-B. Zhang, J. Jiang, W. L. Queen, M. R. Hudson and O. M. Yaghi, *J. Am. Chem. Soc.*, 2014, **136**, 4369–4381.
133 M. Khurana and S. Farooq, *AIChE J.*, 2017, **63**, 2987–2995.
134 Z. Hu, Y. Wang, B. B. Shah and D. Zhao, *Adv. Sustainable Syst.*, 2019, **3**, 1800080.
135 Y. Wang, Z. Hu, T. Kundu, Y. Cheng, J. Dong, Y. Qian, L. Zhai and D. Zhao, *ACS Sustainable Chem. Eng.*, 2018, **6**, 11904–11912.
136 P. J. Milner, J. D. Martell, R. L. Siegelman, D. Gygi, S. C. Weston and J. R. Long, *Chem. Sci.*, 2018, **9**, 160–174.
137 J.-H. Lee, R. L. Siegelman, L. Maserati, T. Rangel, B. A. Helms, J. R. Long and J. B. Neaton, *Chem. Sci.*, 2018, **9**, 5197–5206.
138 M. E. Davis and R. J. Davis, *Fundamentals of Chemical Reaction Engineering*, Dover Publications, 2013.
139 F. Stallmach and J. Kärger, *Adsorption*, 1999, **5**, 117–133.
140 Y. Wang and D. Zhao, *Cryst. Growth Des.*, 2017, **17**, 2291–2308.
141 L. Li, J. G. Bell, S. Tang, X. Lv, C. Wang, Y. Xing, X. Zhao and K. M. Thomas, *Chem. Mater.*, 2014, **26**, 4679–4695.
142 P. Nugent, Y. Belmabkhout, S. D. Burd, A. J. Cairns, R. Luebke, K. Forrest, T. Pham, S. Ma, B. Space, L. Wojtas, M. Eddaoudi and M. J. Zaworotko, *Nature*, 2013, **495**, 80–84.
143 C. Y. Lee, Y.-S. Bae, N. C. Jeong, O. K. Farha, A. A. Sarjeant, C. L. Stern, P. Nickias, R. Q. Snurr, J. T. Hupp and S. T. Nguyen, *J. Am. Chem. Soc.*, 2011, **133**, 5228–5231.
144 K. Li, D. H. Olson, J. Seidel, T. J. Emge, H. Gong, H. Zeng and J. Li, *J. Am. Chem. Soc.*, 2009, **131**, 10368–10369.
145 S. Tanaka, K. Fujita, Y. Miyake, M. Miyamoto, Y. Hasegawa, T. Makino, S. Van der Perre, J. C. S. Remi, T. Van Assche, G. V. Baron and J. F. M. Denayer, *J. Phys. Chem. C*, 2015, **119**, 28430–28439.
146 B. K. Sward and M. D. LeVan, *Adsorption*, 2003, **9**, 37–54.
147 T. M. Tovar, J. Zhao, W. T. Nunn, H. F. Barton, G. W. Peterson, G. N. Parsons and M. D. LeVan, *J. Am. Chem. Soc.*, 2016, **138**, 11449–11452.
148 B. M. Connolly, D. G. Madden, A. E. H. Wheatley and D. Fairen-Jimenez, *J. Am. Chem. Soc.*, 2020, **142**, 8541–8549.
149 B. M. Connolly, M. Aragones-Anglada, J. Gandara-Loe, N. A. Danaf, D. C. Lamb, J. P. Mehta, D. Vulpe, S. Wuttke, J. Silvestre-Albero, P. Z. Moghadam, A. E. H. Wheatley and D. Fairen-Jimenez, *Nat. Commun.*, 2019, **10**, 2345.
150 S. Lawson, C. Griffin, K. Rapp, A. A. A. Rownaghi and F. Rezaei, *Energy Fuels*, 2019, **33**, 2399–2407.
151 J. M. Tuffnell, C. W. Ashling, J. Hou, S. Li, L. Longley, M. L. Ríos Gómez and T. D. Bennett, *Chem. Commun.*, 2019, **55**, 8705–8715.
152 A.-M. Banu, D. Friedrich, S. Brandani and T. Düren, *Ind. Eng. Chem. Res.*, 2013, **52**, 9946–9957.
153 A. Samanta, A. Zhao, G. K. H. Shimizu, P. Sarkar and R. Gupta, *Ind. Eng. Chem. Res.*, 2012, **51**, 1438–1463.
154 C. P. O'Brien, *J. Membr. Sci.*, 2021, **619**, 118751.
155 M. O. Guerrero-Pérez and M. A. Bañares, *Catal. Today*, 2006, **113**, 48–57.
156 T. Hartman, R. G. Geitenbeek, C. S. Wondergem, W. van der Stam and B. M. Weckhuysen, *ACS Nano*, 2020, **14**, 3725–3735.
157 B. M. Weckhuysen, *Phys. Chem. Chem. Phys.*, 2003, **5**, 4351.
158 J.-D. Grunwaldt, J. B. Wagner and R. E. Dunin-Borkowski, *ChemCatChem*, 2013, **5**, 62–80.
159 V. Bon, E. Brunner, A. Pöppl and S. Kaskel, *Adv. Funct. Mater.*, 2020, **30**, 1907847.
160 K. I. Hadjiivanov, D. A. Panayotov, M. Y. Mihaylov, E. Z. Ivanova, K. K. Chakarova, S. M. Andonova and N. L. Drenchev, *Chem. Rev.*, 2021, **121**(3), 1286–1424.
161 Y. Fu, H. Guan, J. Yin and X. Kong, *Coord. Chem. Rev.*, 2021, **427**, 213563.
162 T. L. Easun, F. Moreau, Y. Yan, S. Yang and M. Schröder, *Chem. Soc. Rev.*, 2017, **46**, 239–274.
163 L. Braglia, E. Borfecchia, L. Maddalena, S. Øien, K. A. Lomachenko, A. L. Bugaev, S. Bordiga, A. V. Soldatov, K. P. Lillerud and C. Lamberti, *Catal. Today*, 2017, **283**, 89–103.
164 M. A. Soldatov, A. Martini, A. L. Bugaev, I. Pankin, P. V. Medvedev, A. A. Guda, A. M. Aboraia, Y. S. Podkovyrina,

A. P. Budnyk, A. A. Soldatov and C. Lamberti, *Polyhedron*, 2018, **155**, 232–253.
165 P. L. Llewellyn, S. Bourrelly, C. Vagner, N. Heymans, H. Leclerc, A. Ghoufi, P. Bazin, A. Vimont, M. Daturi, T. Devic, C. Serre, G. De Weireld and G. Maurin, *J. Phys. Chem. C*, 2013, **117**, 962–970.
166 Y. Lu, B. E. G. Lucier, Y. Zhang, P. Ren, A. Zheng and Y. Huang, *Phys. Chem. Chem. Phys.*, 2017, **19**, 6130–6141.
167 M. Mendt, B. Jee, N. Stock, T. Ahnfeldt, M. Hartmann, D. Himsl and A. Pöppl, *J. Phys. Chem. C*, 2010, **114**, 19443–19451.
168 M. Mendt, P. Vervoorts, A. Schneemann, R. A. Fischer and A. Pöppl, *J. Phys. Chem. C*, 2019, **123**, 2940–2952.
169 M. Du, L. Li, M. Li and R. Si, *RSC Adv.*, 2016, **6**, 62705–62716.
170 C. Giacobbe, E. Lavigna, A. Maspero and S. Galli, *J. Mater. Chem. A*, 2017, **5**, 16964–16975.
171 L. Wang, L. Wang, J. Zhang, X. Liu, H. Wang, W. Zhang, Q. Yang, J. Ma, X. Dong, S. J. Yoo, J.-G. Kim, X. Meng and F.-S. Xiao, *Angew. Chem., Int. Ed.*, 2018, **57**, 6104–6108.
172 A. Ramirez, L. Gevers, A. Bavykina, S. Ould-Chikh and J. Gascon, *ACS Catal.*, 2018, **8**, 9174–9182.
173 J. Wei, Q. Ge, R. Yao, Z. Wen, C. Fang, L. Guo, H. Xu and J. Sun, *Nat. Commun.*, 2017, **8**, 16170.
174 L. Jiao, W. Yang, G. Wan, R. Zhang, X. Zheng, H. Zhou, S. Yu and H. Jiang, *Angew. Chem., Int. Ed.*, 2020, **59**, 20589–20595.
175 Y. Gong, L. Jiao, Y. Qian, C. Pan, L. Zheng, X. Cai, B. Liu, S. Yu and H. Jiang, *Angew. Chem., Int. Ed.*, 2020, **59**, 2705–2709.
176 T. Stroud, T. J. Smith, E. Le Saché, J. L. Santos, M. A. Centeno, H. Arellano-Garcia, J. A. Odriozola and T. R. Reina, *Appl. Catal., B*, 2018, **224**, 125–135.
177 L. Yang, L. Pastor-Pérez, S. Gu, A. Sepúlveda-Escribano and T. R. Reina, *Appl. Catal., B*, 2018, **232**, 464–471.
178 C.-A. H. Price, L. Pastor-Pérez, T. Ramirez Reina and J. Liu, *React. Chem. Eng.*, 2018, **3**, 433–436.
179 L. Pastor-Pérez, V. Patel, E. Le Saché and T. R. Reina, *J. Energy Inst.*, 2020, **93**, 415–424.
180 W.-G. Cui, G.-Y. Zhang, T.-L. Hu and X.-H. Bu, *Coord. Chem. Rev.*, 2019, **387**, 79–120.
181 W. Xu, K. B. Thapa, Q. Ju, Z. Fang and W. Huang, *Coord. Chem. Rev.*, 2018, **373**, 199–232.
182 L. Jiao, J. Y. R. Seow, W. S. Skinner, Z. U. Wang and H.-L. Jiang, *Mater. Today*, 2019, **27**, 43–68.
183 T. Kitao, Y. Zhang, S. Kitagawa, B. Wang and T. Uemura, *Chem. Soc. Rev.*, 2017, **46**, 3108–3133.
184 W. J. Lee, C. Li, H. Prajitno, J. Yoo, J. Patel, Y. Yang and S. Lim, *Catal. Today*, DOI: 10.1016/j.cattod.2020.02.017.
185 C. Vogt, M. Monai, G. J. Kramer and B. M. Weckhuysen, *Nat. Catal.*, 2019, **2**, 188–197.
186 J. B. Cohen and H. D. Dakin, *J. Chem. Soc., Trans.*, 1902, **81**, 1324–1344.
187 Y. Zheng, H. Liu and Y. Zhang, *ChemSusChem*, 2020, **13**, 6090–6123.
188 B. Miao, S. S. K. Ma, X. Wang, H. Su and S. H. Chan, *Catal. Sci. Technol.*, 2016, **6**, 4048–4058.
189 K. Stangeland, D. Kalai, H. Li and Z. Yu, *Energy Procedia*, 2017, **105**, 2022–2027.
190 W. Li, H. Wang, X. Jiang, J. Zhu, Z. Liu, X. Guo and C. Song, *RSC Adv.*, 2018, **8**, 7651–7669.
191 L. Shen, J. Xu, M. Zhu and Y.-F. Han, *ACS Catal.*, 2020, **10**, 14581–14591.
192 J. Ashok, S. Pati, P. Hongmanorom, Z. Tianxi, C. Junmei and S. Kawi, *Catal. Today*, 2020, **356**, 471–489.
193 J. C. Navarro, M. A. Centeno, O. H. Laguna and J. A. Odriozola, *Renewable Energy*, 2020, **161**, 120–132.
194 M. Younas, L. Loong Kong, M. J. K. Bashir, H. Nadeem, A. Shehzad and S. Sethupathi, *Energy Fuels*, 2016, **30**, 8815–8831.
195 J. H. Kwak, L. Kovarik and J. Szanyi, *ACS Catal.*, 2013, **3**, 2449–2455.
196 G. Zhan and H. C. Zeng, *ACS Catal.*, 2017, **7**, 7509–7519.
197 C.-C. Hou, H.-F. Wang, C. Li and Q. Xu, *Energy Environ. Sci.*, 2020, **13**, 1658–1693.
198 T. Zhang, Z. Chen, A. G. Walsh, Y. Li and P. Zhang, *Adv. Mater.*, 2020, **32**, 2002910.
199 L. Oar-Arteta, T. Wezendonk, X. Sun, F. Kapteijn and J. Gascon, *Mater. Chem. Front.*, 2017, **1**, 1709–1745.
200 R. J. Young, M. T. Huxley, E. Pardo, N. R. Champness, C. J. Sumby and C. J. Doonan, *Chem. Sci.*, 2020, **11**, 4031–4050.
201 R. Lippi, S. C. Howard, H. Barron, C. D. Easton, I. C. Madsen, L. J. Waddington, C. Vogt, M. R. Hill, C. J. Sumby, C. J. Doonan and D. F. Kennedy, *J. Mater. Chem. A*, 2017, **5**, 12990–12997.
202 L. Zeng, Y. Wang, Z. Li, Y. Song, J. Zhang, J. Wang, X. He, C. Wang and W. Lin, *ACS Appl. Mater. Interfaces*, 2020, **12**, 17436–17442.
203 H. Jiang, Q. Gao, S. Wang, Y. Chen and M. Zhang, *J. CO2 Util.*, 2019, **31**, 167–172.
204 Z.-W. Zhao, X. Zhou, Y.-N. Liu, C.-C. Shen, C.-Z. Yuan, Y.-F. Jiang, S.-J. Zhao, L.-B. Ma, T.-Y. Cheang and A.-W. Xu, *Catal. Sci. Technol.*, 2018, **8**, 3160–3165.
205 W. Zhen, F. Gao, B. Tian, P. Ding, Y. Deng, Z. Li, H. Gao and G. Lu, *J. Catal.*, 2017, **348**, 200–211.
206 N. Prinz, L. Schwensow, S. Wendholt, A. Jentys, M. Bauer, W. Kleist and M. Zobel, *Nanoscale*, 2020, **12**, 15800–15813.
207 W. Li, A. Zhang, X. Jiang, C. Chen, Z. Liu, C. Song and X. Guo, *ACS Sustainable Chem. Eng.*, 2017, **5**, 7824–7831.
208 X. Lin, S. Wang, W. Tu, Z. Hu, Z. Ding, Y. Hou, R. Xu and W. Dai, *Catal. Sci. Technol.*, 2019, **9**, 731–738.
209 M. D. Porosoff, B. Yan and J. G. Chen, *Energy Environ. Sci.*, 2016, **9**, 62–73.
210 X. Su, X. Yang, B. Zhao and Y. Huang, *J. Energy Chem.*, 2017, **26**, 854–867.
211 A. Goguet, F. Meunier, J. P. Breen, R. Burch, M. I. Petch and A. Faur Ghenciu, *J. Catal.*, 2004, **226**, 382–392.
212 G. Pekridis, K. Kalimeri, N. Kaklidis, E. Vakouftsi, E. F. Iliopoulou, C. Athanasiou and G. E. Marnellos, *Catal. Today*, 2007, **127**, 337–346.
213 L. Yang, L. Pastor-Pérez, J. J. Villora-Pico, S. Gu, A. Sepúlveda-Escribano and T. R. Reina, *Appl. Catal., A*, 2020, **593**, 117442.

214 N. Nityashree, C. A. H. Price, L. Pastor-Perez, G. V. Manohara, S. Garcia, M. M. Maroto-Valer and T. R. Reina, *Appl. Catal., B*, 2020, **261**, 118241.
215 X. Liu, L. He, Y.-M. Liu and Y. Cao, *Acc. Chem. Res.*, 2014, **47**, 793–804.
216 M. Kandiah, M. H. Nilsen, S. Usseglio, S. Jakobsen, U. Olsbye, M. Tilset, C. Larabi, E. A. Quadrelli, F. Bonino and K. P. Lillerud, *Chem. Mater.*, 2010, **22**, 6632–6640.
217 L. Chen, Y. Peng, H. Wang, Z. Gu and C. Duan, *Chem. Commun.*, 2014, **50**, 8651.
218 M. Ranocchiari and J. A. van Bokhoven, *Phys. Chem. Chem. Phys.*, 2011, **13**, 6388.
219 Y. Li, P. Song, J. Zheng and X. Li, *Chem. – Eur. J.*, 2010, **16**, 10887–10892.
220 H. Xu, Y. Li, X. Luo, Z. Xu and J. Ge, *Chem. Commun.*, 2017, **53**, 7953–7956.
221 Q. Zhang, L. Pastor-Pérez, W. Jin, S. Gu and T. R. Reina, *Appl. Catal., B*, 2019, **244**, 889–898.
222 Z. Zheng, H. Xu, Z. Xu and J. Ge, *Small*, 2018, **14**, 1702812.
223 E. S. Gutterød, S. Øien-Ødegaard, K. Bossers, A.-E. Nieuwelink, M. Manzoli, L. Braglia, A. Lazzarini, E. Borfecchia, S. Ahmadigoltapeh, B. Bouchevreau, B. T. Lønstad-Bleken, R. Henry, C. Lamberti, S. Bordiga, B. M. Weckhuysen, K. P. Lillerud and U. Olsbye, *Ind. Eng. Chem. Res.*, 2017, **56**, 13206–13218.
224 E. le Saché, L. Pastor-Pérez, B. J. Haycock, J. J. Villora-Picó, A. Sepúlveda-Escribano and T. R. Reina, *ACS Sustainable Chem. Eng.*, 2020, **8**, 4614–4622.
225 A. Dhakshinamoorthy, A. M. Asiri and H. Garcia, *ACS Catal.*, 2017, **7**, 2896–2919.
226 S. Dang, Q.-L. Zhu and Q. Xu, *Nat. Rev. Mater.*, 2018, **3**, 17075.
227 M. Ronda-Lloret, S. Rico-Francés, A. Sepúlveda-Escribano and E. V. Ramos-Fernandez, *Appl. Catal., A*, 2018, **562**, 28–36.
228 J. Zhang, B. An, Y. Hong, Y. Meng, X. Hu, C. Wang, J. Lin, W. Lin and Y. Wang, *Mater. Chem. Front.*, 2017, **1**, 2405–2409.
229 L. Karam, J. Reboul, S. Casale, P. Massiani and N. El Hassan, *ChemCatChem*, 2020, **12**, 373–385.
230 R. Vakili, R. Gholami, C. E. Stere, S. Chansai, H. Chen, S. M. Holmes, Y. Jiao, C. Hardacre and X. Fan, *Appl. Catal., B*, 2020, **260**, 118195.